CR 114635

AVAILABLE TO THE PUBLIC

[redacted]

(NASA-CR-114635) SOLAR FLARE PREDICTIONS AND WARNINGS Final Report (Aerospace Corp., El Segundo, Calif.) 74 p HC $5.75 68 CSCL 03B

N73-31707

Unclas

G3/29 13502

THE AEROSPACE CORPORATION

SOLAR FLARE PREDICTIONS AND WARNINGS: FINAL REPORT

Prepared by

K. P. White, III and E. B. Mayfield

July 6, 1973

Prepared for
National Aeronautics and Space Administration
Ames Research Center
Moffett Field, California

Contract No. NAS2-7292

Abstract

A description of the work performed under the contract "Solar Flare Predictions and Warnings" is presented. Included in the summaries of effort are the real-time solar monitoring information supplied to support SPARCS-equipped rocket launches, the routine collection and analysis of 3.3-mm solar radio maps, short-term flare forecasts based on these maps, longer-term forecasts based on the recurrence of active regions, and results of the synoptic study of solar active regions at 3.3-mm wavelength.

In excess of 80% of the 24-hr forecasts calling for flare activity materialized in a flare, as shown in the following table summarizing the results:

	flare≥ 1N occurred	flare≥ 1N did not occur	forecast success
flare was forecast	13	3	81%
flare was not forecast	12	400	97%

The 28-day forecasts were particularly successful, for example, in correctly anticipating the possibility of flare activity from the highly-publicized active center of the first week of August, 1972. This center of activity was preceded in location by seven notable flare-producing regions dating back to June, 1970.

Synoptic radio maps at 3.3-mm wavelength are presented for twenty-three solar rotations in 1967 and 1968, as well as synoptic flare charts for the same period. Among the results of the synoptic study, we can list:

1) the millimeter enhancements consist of a facular-related component and a sunspot component
2) it is the sunspot component which produces the peak

enhancement which correlates well with flare productivity

3) active regions exhibiting millimeter enhancements less than 4.5% of the quiet sun level will not produce flares because of the inferred lack of sufficiently developed sunspots.

CONTENTS

ABSTRACT i

INTRODUCTION 1

TASK I 1

TASK II 2

TASK III 6

TASK IV 7

1. Introduction 7
2. Compilation of the Synoptic Maps 8
3. Advantages of the Synoptic Presentation 11
4. Analysis of the Synoptic Maps 12
   - A. Longevity 12
   - B. Comparisons with Other Synoptic Data . 13
5. Conclusions 20

REFERENCES 23

GLOSSARY 24

FIGURE CAPTIONS 27

FIGURES 1-9 29

APPENDIX A 38

APPENDIX B 51

Introduction

This report summarizes effort on the contract NAS2-7292 "Solar Flare Predictions and Warnings" for the period of 6 July 1972 to 1 July 1973. The efforts under this contract are in support of launches of solar research sounding rockets whose stabilization is achieved by a SPARCS pointing system provided by the NASA Ames Research Center. The total effort has been divided into four separate tasks, the first three of which are operationally oriented toward providing solar information to rocket launch teams, while the fourth is an analysis-research task to improve and extend the capability to provide the information under the other three tasks. Progress on each task will be outlined individually by task.

Task I

Task I, "Flare Prediction and Launch Support," whose objective is to provide information about the condition of the solar disk to permit the timely preparation and exact launch time for a sounding rocket payload, has been exercised in support of the launch by the Loren Acton group (Lockheed, Palo Alto) from WSMR on 18 January, 1973. A long-range forecast to expect increased solar activity for a few days centered around 18 January 1973 was relayed to R. Catura (Lockheed, Palo Alto) on 19 December 1972. With this information, range time was scheduled and a launch by Acton and his group was performed at 1755 UT on 18 January 1973. Due to a long-enduring rainstorm in the Los Angeles area, no real time information could be relayed to the launch crew. In fact, no Hα filtergrams were taken on the day of the launch nor on the preceding or following day. No reliable 3-mm radio map had been obtained on the previous five days due to the weather, but that obtained on 19 January is being relayed to Catura for his use in data analysis. No other requests for support under Task I were received.

Task II

"Routine Solar Observations of Flares and Predictions," task II, requires that The Aerospace Corporation shall obtain daily isotherm maps of the sun at a wavelength of 3.3 mm. From these data flare probabilities are to be calculated according to the method developed by White (1972), which is based upon the peak temperature enhancement measured at 3.3 mm and the history of recurrence of flare activity for given active regions. The results of this effort are presented in Tables I and II.

Table I: Regions with reliable pre-flare maps which did flare.

McMath region #	time of map (hrs. before flare)	% probability of 1N	1B	flare class
11939	10-15	23	22	1N, 1N
947	14	12	12	1N
949	15	32	31	1N
	41	29	28	1B
	17	63	50	1N
957	32	2	nil	1N
	14	84	65	1B
970	38	52	44	1B
976	36-48	100	95	1B, 1N, 3B
12001	27	19	18	1N
	6	64	53	1N
002	13	100	76	2B
044	53	100	71	1B
056	28	3	nil	1B
094	1-46	86	63	1N, 1B, 1B, 1N
	37	100	100	1B
	20	100	72	1B
115	10	32	31	1B
136	33	32	31	1B
164	19	53	46	1N
228	27	nil	nil	1B
205	14	6	6	1B
259	11	10	10	1N
306	24	80	63	1B
336	2-11	100	100	1N, 2B

Table II: Regions with temperature enhancements ≥ 7% (indicating ≥ 50% chance of flaring) which did not flare.

McMath region #	% probability of 1N	1B
11965	55	47
968	nil	nil
986	nil	nil
12007	89	65
028	nil	nil
039	nil	nil
085	nil	nil
086	nil	nil
114	nil	nil
207	59	50

Table I lists all McMath plage regions observed at 3.3-mm wavelength from 1 July 1972 - 15 May 1973 which did produce one or more flares of class ≥1N. Included here are only those regions which were reliabily measured prior to a flare, that is, within not more than two days preceding a flare and not beyond 60° longitude from the central meridian of the solar disk. Weather conditions could not have been foggy or rainy, either. Table I contains the regions listed by McMath plage number, the number of hours prior to the flare that the map was made, the percent probability of occurrence of a class 1N flare and a class 1B flare as determined from the radio measurements (according to White, 1972), and the flares of class ≥1N which were reported within two days of the radio map. Table II lists any regions which attained a peak temperature enhancement ≥7% (indicating a 50% chance or greater of flaring), but in this case did not produce a reported flare of class ≥1N. All but three of the regions listed in Table II indicated a nil probability of a class 1N flare, due to the fact that they were designated "virgin regions," indicating lack of a history of recurrent flare activity, as developed by White (1972).

The interpretation of the results tabulated in Tables I and II indicates a good measure of success for the flare forecast method developed by White (1972). During the 10.5-month period of study, slightly more

than 400 plage regions were assigned McMath plage numbers (#11939-#12349); this constitutes the entire sample of possible flare-producing regions. Thirty-two flares, as listed in Table I, were preceded by twenty-five reliable radio map measurements. The results can be summarized in Table III:

Table III: Forecast summary for flares of class ≥ 1N. All data are drawn from Tables I and II.

	flare ≥1N occurred	flare ≥1N did not occur	forecast success rate
1N flare prediction ≥50%	13	3	81%
1N flare prediction <50%	12	400	97%

These results are interpreted by reading across the rows. For example, of the 16 predictions that flares would occur (13 in Table I, 3 in Table II), i.e., the 1N flare prediction ≥50%, 13 flares materialized while 3 failed to materialize, for a success rate of 81%. Of the approximately 400 regions which did not result in a class 1N flare prediction of 50%, only 12 flares were subsequently reported (Table I), for a success rate of 97%.

These results provide further insight into the ability to forecast flare activity under task II, since they constitute the first test of the method developed by White (1972). First of all, the fact that 52% of the flares which occurred had flare predictions of 50% or greater, and 48% had less than a 50% prediction, only indicates that about half the flares occur in regions of ≥7% peak enhancement, while about an equal number occur in less enhanced regions. The apparent 52% success rate of predicting flares that occurred is entirely determined by what threshold is chosen (in the present case, 50%), and should, therefore, not be interpreted as a measure of merit. It is more important to realize that the mean

prediction probability for the 13 regions listed in Table I, which were predicted to flare, is 83%. This compares very favorably with the 81% of the positive flare predictions which did materialize in flares and must be regarded as strong confirmation of the flare forecast method. In other words, the observed rate of occurrence (81%) was equal to the average predicted rate of occurrence (83%), within the errors of uncertainty; the quoted forecast probability for flaring was accurate.

Finally, it is worthwhile to review the forecasting success of the present work within the context of other forecast performance. Simon and McIntosh (1972) have made a survey of current solar forecast centers and conclude that solar forecasts are most accurate when quiet conditions are predicted, but the greatest skill is shown when forecasting the most energetic flares and proton events. To summarize their findings, high accuracy can result from the dominance in frequency of occurrence of a certain condition and, therefore, may not be much of an indication of skill. For instance, 97% of all the forecasts for quiet conditions were correct. Simon and McIntosh state that quiet conditions can be forecast with up to 90% accuracy, based on the forecast experiences at the NOAA Space Environment Forecast Center in Boulder and the Observatoire de Paris at Meudon. On the other hand, skill is demonstrated by the ability to forecast rarer events accurately, up to 40% accuracy according to Simon and McIntosh. In the case of the present work, 81% accuracy was attained for a given positive forecast (of 83% average probability), numbers indicative of considerable skill in light of the difficulties experienced by all forecasters.

Further insight into the critical review conducted by Simon and McIntosh (1972) is provided by two companion articles by Lemmon (1972) and Smith (1972) which describe some of the details of the forecasting techniques employed at NOAA-Boulder on a regular basis and on an experimental basis. Lemmon's work was of an experimental nature involving flare forecasting based on the number of inflection points of the longitudinal magnetic field neutral line in an active region, the

horizontal gradient of the longitudinal magnetic field, and the time rate of change of this last parameter. The technique appeared successful at first but further use revealed some inconsistencies requiring more study, so it is not currently incorporated in formulating the NOAA forecasts. On the other hand, Smith (1972) discusses prediction of activity levels for specific locations within active regions. The methodology and performance are reviewed for this technique of forecasting flare location region by region, which, to a large degree, continues to be employed in formulation of the NOAA forecasts. These forecasts are based on more subjective inputs than the 3.3-mm method, but the wealth of observer experience coupled with a wide variety of observations has resulted in a success rate approaching 60%.

Task III

The long-term forecasts of task III, of 28 days duration and 4 months duration, have been delivered periodically to the Technical Monitor. The flare-record chart, from which the forecasts are compiled, has been maintained and updated; it is presented in Figure 1 in the same format as presented in White (1972), to which the reader is referred for details. The small squares entered in the most recent portion of the chart indicate preliminary flare centers through 15 May 1973. It is significant that the more energetic flare regions do continue to cluster around these trend lines which were originally drawn in July 1971 and extrapolated since then. Of particular interest on this chart is the correct anticipation of flare activity from region #11976 (central meridian passage on 4 August 1972), the highly publicized center of considerable flare activity during the first week of August, 1972. This active region was located at N13°. Tracing back along its trend line, we see this region was preceded by regions at N13°, 11°, 15°, 13°, 8°, 13°, and 10°, all the way back to June 1970, truly a remarkable example of a long-lived active region.

Task IV: Synoptic Study of Solar Active Regions at Millimeter Wavelengths

I. Introduction

The solar flare phenomenon has been identified historically as a short-lived increased brightness emanating from a local region in the low solar atmosphere, a definition resulting directly from the first observational procedures used in studying the sun. Such observations of flares in various solar absorption lines (especially Hα) continue to today, of course, and still provide the highest spatial resolution with which flares can be recorded. Advances within the fields of solar physics and space research in the past two decades have provided the capability to observe the sun in parts of the energy spectrum in which man was theretofore blind. In particular, observations of the sun can now be made at frequencies of gamma-rays, x-rays, ultraviolet light, far infrared light, at short and long radio wavelengths, and of the particle radiation, either directly (in space) or indirectly through the influences on the terrestrial atmosphere (aurorae, sudden ionospheric disturbances) and magnetosphere (magnetic storms).

Optical observations of flares in the light of Hα remain the most common way that solar physicists relate to flares, but the expanded view across the spectrum has revealed that the expression of the flare as an Hα brightening may be overshadowed in a number of respects by other expressions of the phenomenon. For example, the total energy released during a flare as measured in the Hα spectrum line is matched by the total emission in x-rays from 8-12Å, each of which accounts for about 10% of the total flare energy release (Thomas and Teske, 1971). Furthermore, the bulk of the flare energy is thought to go into the interplanetary plasma cloud (de Jager, 1970; Bruzek, 1967), so that in true perspective, the Hα manifestation of a solar flare can be likened to the match that lights a fireplace.

In addition to the energy release in the Hα spectrum line's

being eclipsed, the relative increase in brightness, i.e. the intensity during a flare versus the pre-flare intensity, can be much greater in other parts of the spectrum than observed in Hα. For example, the Hα intensity rarely increases by a factor of 10, usually not more than a factor of about 5, while flaring as observed in the 1-8Å band or at radio wavelengths from cm to m can increase by factors of 1000 or 10,000. This evidence is presented not to diminish the importance of Hα observations of flares but instead to illustrate the dynamic effects which have yet to be so thoroughly investigated and analyzed at other wavelengths.

The present work is an investigation of the properties of solar active regions at a radio wavelength of 3.3-mm. From previous studies some important information is already known about the region of the solar atmosphere which one studies at 3.3-mm. In particular, from the work done by Shimabukuro (1970), we know that most of the central disk 3.3-mm emission comes from a thin layer of relatively constant temperature about 1500-3500 km above the photosphere, i.e. in the low chromosphere. Furthermore, the temperature of the region responsible for the mm emission has also been calculated. Until recently, the value adopted has been very nearly 6600 K, as found, for example, by Reber (1971) who obtained a value of 6646±135K. In a recalibration of the quiet sun millimeter spectrum, placing a large number of solar millimeter observations on a common scale, Linsky (1973) has obtained a value for the temperature of 7464±~100K. In this work we will adopt a value of 7500K for the temperature of the quiet sun at the disk center at 3.3-mm wavelength.

The equipment used for all of the radio observations is the 15-ft diameter radio telescope of The Aerospace Corporation. Operation of this instrument to obtain full disk solar radio maps has been described in detail elsewhere (Shimabukuro, 1968) and will not be repeated here.

II. Compilation of the Synoptic Maps

Since 1966 solar radio maps at 3.3-mm wavelength have been made at The Aerospace Corporation on most days of the year when weather

permitted. Some additional days have been missed due to equipment down-time. These solar maps, starting with January, 1967, constitute the library of data for compilation of the synoptic radio maps.

Examples of twenty-four consecutive solar rotations are presented in Appendix A as Figures 10 through 21. With reference to these figures, their method of construction and symbols will be explained. First of all, each map represents one rotation period of the sun about its axis. Since the sun's rotation rate is known to decrease with increasing heliographic latitude and, furthermore, even appears non-uniform ("jerky") at a given latitude due to proper motions of various surface features, a mean rotation rate had to be selected. This was actually done years ago by Carrington in England, and we have adopted his system, which is quite common in solar research. Accordingly, each of the maps is labeled with the Carrington rotation number (starting with 1516 in late December, 1966) so that it can easily be identified with other types of solar data collected during this period. Running across the middle of each map is the solar equator. Above and below the equator, solar latitudes to 50° north and 50° south are presented. Poleward of these latitudes activity is rarely, if ever, observed, hence, such latitudes would only appear blank and are not presented.

Across the top border of each map is indicated the so-called Carrington longitude from 0° - 360°. If one envisions a central meridian, placed over the solar globe as viewed from the earth with the sun rotating beneath this fixed meridian, the rotation of the sun is such that decreasing longitudes are carried successively past the meridian at a rate of about 13.2° per day. This explains why W for west and E for east, signifying the west and east limbs of the sun, have been placed at the right and left extremes of the map. Features on the sun rotate from solar east to solar west.

Of course, at any one time, one can make an observation of the sun and some certain Carrington longitude will correspond to the central meridian on the sun at that time. To indicate this correspondence, running

across the bottom border of each map is a succession of days with time increasing from right to left. The beginning of each Universal Day is signified by a black dot and the months are indicated by Roman numerals just below the days. By reading vertically to the top border, one can determine the Carrington longitude at the central meridian for any time during each solar rotation. The small vertical lines along the lower border indicate the UT times when solar radio maps were made which are used in the compilation.

With the format of the maps thus understood, we can proceed to an explanation of the data being displayed. It will be recalled that each daily solar map consists of a 19 x 19 grid of radio temperature measurements across the solar disk. There is no daily absolute calibration available, so the point by point readings of each of the maps is calibrated relative to a quiet region of the solar disk. This normalization is done with reference to daily maps of the Fraunhofer Institute in order to avoid normalizing to a region containing $H\alpha$ filament material, which has been shown to be in absorption (Kundu, 1970), hence producing anomalously low temperature measurements at the normalization point and anomalously high relative readings at all other points. Another complication could be the influence of coronal holes on the normalization reading. Coronal holes (Munro and Withbroe, 1972) are characterized as being regions of low coronal electron density, and at least one well-defined hole of 15 November 1967 appears plainly at 3.3-mm and coincides with the normalization point for that date. Whether or not coronal holes invalidate the normalization procedure is not known; in fact, coronal holes may actually overlie truly quiet solar regions and be the most appropriate normalization regions one could choose. Each normalization point is indicated in the synoptic maps by a small cross. In many instances, the normalization points for consecutive maps are coincident or nearly coincident (within the size of the cross), and in such cases a single cross represents more than one normalization point.

Finally, we move on to a discussion of the contours themselves. The enhancement contours are drawn at levels of 4, 6, 8%, etc., above the chosen normalization point and represent the appearance of the regions from a number of daily maps (when possible), weighted most heavily toward the appearance of each region when nearest to the central meridian on the solar disk. Additionally, daily maps made within 6-8 hours after a flare of class ≥1B have been avoided for the region where the flare occurred. Within each peak contour, the peak enhancement has been indicated as it was measured on a daily map. In other words, there has been no interpolation or extrapolation in determining the peak enhancement.

III. Advantages of the Synoptic Presentation

With the collection of solar radio maps on most days of the year and more than one map on some days, the accumulation of data eventually becomes cumbersome to interpret. For this reason, the summarization of large amounts of daily data by means of synoptic charts is a real benefit and necessity. At little more than a glance then, one can locate the millimeter data pertinent to some specific active region he might be studying. Furthermore, the synoptic presentation can be an aid to revealing long-term phenomena which would, otherwise, go unnoticed. For example, the longevity of active regions at millimeter wavelengths can be investigated as well as rotation rates of the millimeter features. More will be said about the former aspect later.

Some of the most significant physics concerning the development of active regions is expected to result from the comparison of these synoptic maps with synoptic maps of other types of solar phenomena. Such comparisons form the substance of the analysis of the present work and have their greatest impact in helping to understand some of the average parameters characterizing active regions. Most importantly, the millimeter radio observations can serve as observed boundary conditions for models constructed on the basis of other, higher resolution (optical) data.

IV. Analysis of the Synoptic Maps

A. Longevity

The question of the longevity of active regions can be investigated by inspection of successive synoptic maps to note the recurrence or lack of recurrence of given active regions. In this respect it is important to point out the sensitivity and precision of the data contained in the synoptic maps, because these parameters will directly influence the visibility of the enhancements. As stated before, the lowest contour level plotted corresponds to a 4% enhancement, so chosen because at this level individual active regions are usually discernable, whereas a 3% contour usually will run nearly the whole length of the map, providing very little information. Additionally, the repeatability of measurements made on different daily maps either on the same day or different days can be as large as $\pm 0.5\%$, though the average is probably closer to $\pm 0.3\%$, with some outstanding examples showing variations of no more than $\pm 0.2\%$ over a five or six-day period. To maintain a precision of about 10% (e.g. $4 \pm 0.4\%$), we felt it was safest to display the 4% contour as the lowest level.

Therefore, the longevity of an active region is defined as the time from when it first exceeded 4% enhancement to when it first disappeared below the 4% level. In this context, some regions are found to last less than a full solar rotation, while others can persist and be followed over five or six rotations. As will be shown below, this result is entirely consistent with the result that the 4% contour level coincides in shape and location with the facular areas, which have lifetimes that can be as short as a few days or as long as a few solar rotations.

Another feature of the synoptic maps whose longevity can be gauged is the quiet regions, as indicated by the clustering of crosses. The nature of these regions is still in question, but certain examples of them can be followed over three or four rotations.

B. Comparisons with Other Synoptic Data

Daily observations of sunspots and photospheric faculae (a network of bright points surrounding sunspots or groups of sunspots, visible toward the limb) have for many years been presented in synoptic form by Waldmeier of Zurich in the publication Heliographic Maps of the Photosphere. These maps show each sunspot group in the state of its maximum evolution. The umbrae are given as black dots, the penumbrae are shown by their outlines. The faculae are first drawn point by point from the original records and then the outlines of these point fields give the extensions of the facular regions as shown by dashed lines on the maps.

Examples of comparisons of the radio synoptic maps with the heliographic maps of the photosphere are presented in Figs. 2, 3, 4, 5, and 6. During these five solar rotations, one can see at a glance how well the 4% enhancement contours correspond to the extensions of the facular regions. Differences in shape and extent can be attributed to a number of causes, which include: 1) slow, evolutionary changes in the active regions, since the photospheric maps pertain to the maximum development of the regions, while the millimeter maps reflect the appearance closest to central meridian passage; 2) rapid changes in the active regions, as caused by flares, whose residual effects can influence the radio contours (although, such has been allowed for and corrected when possible); 3) selection of an invalid normalization point for a particular daily radio map (e.g., a dark absorption filament), which would cause an apparent "growth" or "contraction" of the enhancement levels, and; 4) the lack of a physical connection between the two phenomena.

The first three points are really just problems of observation and have been accounted for as described previously. The fourth point implies that, to the extent that the two phenomena are physically distinct, one would not expect a correspondence in shape and location. We feel that the striking correspondence evident in comparisons between the two types of maps for all 23 solar rotations we have been able to analyze

speaks loudly for there being a physical connection between the two phenomena. On the basis of these data, we will adopt the view that the facular regions and the millimeter enhancements are manifestations of the same phenomenon in the solar atmosphere; namely, the magnetic fields are responsible for the increased emissions in both cases. A more extensive discussion of the role magnetic fields play in enhanced millimeter emission is provided by Shimabukuro et al. (1973), whose research has contributed to the understanding of the present work. With this view in mind, inspection of Figs. 2 through 6 further reveals that scattered facular regions, with no prominent sunspots, rarely exceed about 5% enhancement. If they do, the cause can usually be attributed to a smattering of small sunspots or pores, not all of which appear on Waldmeier's maps. Furthermore, the peak enhancements more likely than not, will correspond in location to the sunspots, even in active regions not exhibiting much flaring. These observations suggest regarding the measured millimeter enhancements as being made up of two components; one component can be attributed to heating which also manifests itself in the faculae; the other component should be associated with the sunspot magnetic fields and some sort of containment of an excess-heated plasma. The latter component will be discussed in more detail in a later section dealing with flares. The former component will be discussed next.

By inspection, the contours in greatest agreement with the facular areas are the 4% contours. In some cases, a slightly greater contour, perhaps 5%, would produce a cleaner correspondence. In either case, it is clear that most outlying facular regions, uncontaminated by the sunspot component, would lie between the 4% and 5% contours. Thus, we shall adopt a mean enhancement of $4.5\% \pm 0.5$ as representative of the excess heating at 3.3 mm measured by the radio telescope. With the adoption of 7500K as the temperature of the quiet sun, the enhancement above facular regions corresponds to about 340K. Such a measurement must be corrected for the fraction of the radio beam which is actually

being filled by the heated structures. An estimate of such a fraction involves many assumptions about the fine structure of the low chromosphere and an indefensible extrapolation of models of heating in faculae, which models do not extend sufficiently high into the solar atmosphere. Future work could attempt to achieve consonance between the physical parameters indicated by the mm measurements and a facular model, such as that by Chapman (1970), but such is beyond the scope of the present work. For now the correspondence between the 4.5% enhancement at 3.3 mm and faculae can only be substantiated on the basis of spatial coincidence.

There are important consequences for interpretation of the millimeter radio maps resulting from the identification of facular and sunspot components in the enhancements; these will be dealt with in a separate, following section.

A second comparison of the synoptic millimeter radio data can be made with the Hα synoptic charts being produced by McIntosh (1972). See Figs. 7 and 8. These maps depict the large-scale distribution of solar magnetic fields as inferred from the positions of filaments (cross-hatched), plage corridors (solid lines through stippled areas), filament channels (solid lines outside active regions), and sunspots (large dots, drawn schematically). The stippled areas represent the H-alpha plages. Dashed lines are interpolations and estimates required to obtain consistency with polarities and patterns observed on previous solar rotations. The "+" and "-" signs give the polarity of the solar magnetic field. The heliographic latitude is given along the left- and right-hand side of the map, the Carrington longitude is given along the bottom, and the date of the central meridian passage of a given longitude appears at the top.

By using transparent overlays of one map upon the other, the relation of millimeter radio features to Hα and magnetic structures has been investigated. We can summarize our findings with the following list:

1) the enhancements are positioned over regions of magnetic polarity reversal, indicative of the preponderance of bipolar

sunspot groups forming active regions

2) the quiet regions of normalization (crosses) occur generally in the midst of unipolar magnetic regions, which have been characterized as containing open magnetic field line formations and general lack of solar activity

3) perhaps 20% or so of the normalization points fall near enough to filaments, filament channels, or plage corridors that they should be suspect of producing anomalously low normalization readings, even with the care taken to avoid such occurrences, as described previously.

Solar flare data used for comparison with the mm-emission synoptic maps was taken from Solar Geophysical Data of NOAA. The importance assigned by NOAA in the comprehensive volume of the reports was used. In instances where secondary maxima were reported for a single flare event, the greatest classification was adopted. Values of flare importance number given by NOAA are based on measurements of the area of the flare in units of millionths of the solar hemisphere. These numbers and related areas are: subflare, <100; class 1, 100-250; class 2, 250-600; class 3, 600-1200 and class 4, >1200. In addition, flares are characterized as normal (N), faint (F) or bright (B). For this investigation, we have limited the flares to those of importance 1B or greater to limit the number to be plotted.

We have also included the new flare importance number designation proposed by Dodson and Hedeman (1971). This system is based on five criteria for flare importance and gives greater emphasis to x-ray, radio and charged particle emission. Although this method is sensitive to radio (and hence electron) emission, it provides a more quantitative measure of flare importance. The parameters used for this classification are: 1) ionizing radiation, 2) flare importance number, 3) 10-cm (3GHz) radio flux, 4) dynamic radio spectrum and 5) 200-MHz radio flux. Numerical values for this method range from 1 to about 17. We have plotted

only flares with a value of 5 or greater to limit the number of events considered.

The flare data have been plotted on synoptic maps (see Figs. 22-33 in Appendix B) similar to the mm maps. These flare plots show Carrington longitude (and date) and central meridian distance as the abscissa and ordinate, respectively. Flares are located by time of occurrence and meridian distance. Active regions on these plots are straight lines from 90° east to 90° west, covering 180° in Carrington longitude. Location of each center of activity is designated by McMath calcium plage number, latitude and longitude. The plage number and latitude are written near each active region line and the longitude is determined by the value of central meridian passage at the central horizontal line. Northern hemisphere regions are shown as solid lines and southern regions as dashed. Flare designation is as follows: class 1, open circle; class 2, filled circle; class 3, triangle and class 4, square. The Dodson-Hedeman number is given beside each flare. For those flares with an importance number not exceeding 1N but a Dodson-Hedeman numerical value of 5 or greater, an X is shown.

Active regions plotted in this synoptic fashion show a close association with a fixed location during a disk transit. Some regions have more than one active part but these typically remain distinct. These results show that flares are produced by unique areas of centers of activity which retain close association with the magnetic fields of the underlying sunspots. This is an important result and is in disagreement with the widely accepted opinion that flare data are subject to large errors and that both location and times of occurrence are very uncertain. Although this may be true for reports from individual observatories, the mean values reported in Solar Geophysical Data are highly consistent.

Since flares occur in active regions near sunspot groups and the 3.3-mm emission is associated with the facular regions of magnetic fields, there is a correlation of the flares with enhanced mm-regions. This correlation, however, is complex and no simple rules can be stated.

Evidence for two components of the mm-emission can be seen in the maps. One of these is associated with the general magnetic fields in the faculae and accounts for the enhancements of 4 or 5%. This is the slowly varying component and has been shown by Shimabukuro et al. (1973) to be due to magneto-ionic processes in fields. The second component which accounts for the larger, rapidly changing emission is associated with strong fields and occurs near the neutral lines or sheets of these fields. This strong emission is probably caused by currents in the neutral sheet separating fields of the opposite polarity as has been postulated by Syrovatskii (1966) and Jaggi (1963). Various other theories also propose instabilities at the neutral sheets as the mechanism responsible for flares. In each of these, significant heating should occur in the neutral region prior to flare onset.

Centers of activity which produce the greatest number of flares occur in regions of enhanced 3.3-mm emission, typically with enhancements greater than 8%. A distinctive feature of the mm-emission in these centers is that the radio plage is usually small and the thermal gradient is large. The 4% isotherm tends to occur near the maximum of emission. In other centers which may have a large enhancement but produce few or small flares, the 4% isotherm encloses a large area. This indicates that major flare producing regions have concentrated magnetic fields with necessarily large magnetic flux density and associated $\nabla \times H$ current densities. These results are consistent with previous reports that magnetically complex γ-type sunspot groups produce the greatest number of flares.

In the most active regions, the location of the flare centroids is usually near the maximum of the mm-emission. Since the longitude of each active region is very stable during a single transit and the mm regions change slowly, the association of flare centroid and maximum enhancement is close. For less active regions, however, the flare center is frequently located several degrees from the maximum and may be as great as 10 degrees. The mm enhancements in these cases are usually part of a complex region or two regions joined by a common 4% isotherm. This indicates that the stronger magnetic flux of the original sunspot group has

been dissipated into the region marked by faculae and associated with the slowly varying component of the mm emission. Location of the flare centers for these regions is usually within the 5 or 6% isotherm but rarely a flare may occur at the 4% level of the mm maps.

Although all of the centers of activity which flare are associated with an enhanced region of mm emission, the reverse is not true and a few regions with up to 8 or 9% enhancement may not flare. These are typically part of a larger multiple region similar to those which produce a few small flares during a transit. They provide additional information on the kinetic processes in chromospheric magnetic fields which lead to flares and are valuable in critically evaluating flare theories.

Results of this investigation are consistent with hydromagnetic theories of solar flares. These theories assume that magnetic fields in active regions provide the energy released by a flare and that the configuration of the fields determines the instabilities which cause them. On the basis of these theories, the kinetic energy of the flare is derived from annihilation of magnetic fields. This process is believed to occur in the region separating fields of opposite polarity where electromagnetic theory predicts currents will exist. Several mechanisms have been proposed to account for the field annihilation but each suffers from the defect that calculated times of converting magnetic to kinetic energy are too long. Although this theoretical problem has not been solved, the model is regarded as correct and able to explain all of the observed flare phenomena. Heating of the chromosphere near the neutral region is a result of the electromagnetic currents and is responsible for the enhanced emission in the mm radio. Since this heating is strongly associated with flares it is evident that magnetic field configurations which lead to strong gradients and curl are important to subsequent flares. From the correlations between the mm maps and active flare regions, it is apparent that complex fields with high flux concentration produce the hottest mm regions and the greatest number of flares.

Since the estimated energy required for a major flare

(importance 4) is about 10^{32} ergs, the available magnetic energy in the flare volume must equal or exceed this. From estimates of flare energy made by Thomas and Teske (1971), flares of importance 3 release about 10^{31} ergs, importance 2 about 10^{30} ergs, etc. This permits an estimate to be made of the maximum size flare which can be expected to occur in an active region. Measurements of the total magnetic flux in an active area together with the mm radio emission will provide an improved estimate of flare forecasts.

Finally, a fourth comparison was anticipated with the synoptic charts of solar magnetic fields from Mt. Wilson Observatory, as published in the International Astronomical Union Quarterly Bulletin on Solar Activity. Unfortunately, the data covering the period 1967-8 were omitted from publication originally and are due to be published now but have not yet appeared. These maps contain quantitative information about magnetic field strengths, unlike McIntosh's maps which provide solely positional information about large-scale magnetic features. These maps will be especially useful in eventual quantitative estimates of the magnetic energy residing in active regions.

V. Conclusions

On the basis of the results presented in the previous section, we can conclude that the temperature enhancements we observe at 3.3 mm and from which we can forecast flare probabilities, consist of two components, one associated with the photospheric faculae, the other due to the sunspot magnetic fields. With this view in mind, we can understand why the millimeter enhancements can precede and outlast flaring. When an active region is young, still devoid of sunspots, it will have the appearance of scattered chromospheric plage, corresponding to scattered photospheric facular network. Millimeter enhancements can be observed at this stage at the 4-5% level, due entirely to the facular component. When sunspots begin to appear, the observed enhancement can increase, due to the addition of the sunspot component. As we have shown before,

continued increased heating is correlated to the eventual production of flares, which heating we can now attribute to the magnetic development of complex sunspot structures. Present theories of solar flares, with few exceptions, assume that the energy released by the flare is supplied by magnetic fields in active regions. The exact mechanism for annihilation of the fields is not known, but it is assumed to occur in the neutral line of the fields. Prior to the flare it is this region which is hottest, and the heating is believed to be caused by currents in the neutral region. After the flare, heating continues in the region as a result of hot plasma trapped by the magnetic fields.

The two-component model evolving from this research has consequences for flare forecasting. The energy source for solar flares is contained in the sunspot magnetic fields. Therefore, in those active regions not exhibiting enhancements above about 4.5%, one can infer that sunspots are absent, hence, flares would not be expected. Furthermore, in any analysis of flare production and millimeter heating, corrections of 4.5% should be applied to the observed peak enhancement to account for the facular component which is mixed into the measurement but does not contribute to the flare probability. In other words, the ratios of flare potential from two regions measuring 10% and 6% peak enhancement should not be thought of as 10:6, but instead as 5.5:1.5.

The two-component model also explains some of the results reported on before (White, 1972) in further support of the applicability of the forecast method. Presented in Fig. 9 is a plot taken from White (1972) showing the probability of occurrence of a class 1N flare within a one to two day period vs. the peak temperature enhancement at 3.3. mm. An extrapolation of the curve to lower probabilities would result in about a 4-5% peak enhancement for zero probability of a flare. Before, we had no explanation for this value of the intercept; now we understand it in terms of the sunspot and facular components. Heating of only 4-5% represents the facular component only, no sunspot component, hence, no chance for a flare.

Progress in many areas of solar physics research relies on cooperative sharing of data. In this vein synoptic data are especially valuable for comparison with a variety of data. We, therefore, intend to seek the broadest dissemination of the synoptic millimeter maps as possible to benefit solar research and have made preliminary arrangements for eventual publication of the maps as a UAG report published by NOAA of the Department of Commerce.

Finally, we must point out the direction that the present research indicates to be fruitful for future research. The two-component contributions to the millimeter enhancements suggest the importance of magnetic fields to the heating, since the two components are largely differentiated according to field strength. We, therefore, feel that analysis of the millimeter maps with corresponding quantitative magnetic field data will permit relating the source of the flare energy (the amount available in the form of magnetic fields) to the energy released during a flare event. Calculations of the total magnetic flux in an active region, in addition to field gradients in the neutral line area and temporal changes as employed by Lemmon (1972), can be combined with the millimeter maps to provide estimates of flare probability, location, and importance.

REFERENCES

Bruzek, A.: 1967, in J. N. Xanthakis (ed.), Solar Physics (Interscience Publ., London), p. 399.

Chapman, G. A.: 1970, Solar Phys. 14, 315.

de Jager, C.: 1970, in V. Manno and D. E. Page (eds.), Intercorrelated Satellite Observations Related to Solar Events (Springer-Verlag, New York), p. 25.

Dodson, H. W., and Hedeman, E. R.: 1971, "An Experimental, Comprehensive Flare Index," Report UAG-14, World Data Center A, NOAA, U. S. Dept. of Commerce.

Jaggi, R. K.: 1963, J. Geophys. Research 68, 4429.

Lemmon, J. J.: 1972, in P. S. McIntosh and M. Dryer (eds.), Solar Activity Observations and Predictions (MIT Press, Cambridge, Mass.), p. 421.

Linsky, J. L.: 1973, Solar Phys. 28, 409.

McIntosh, P. S.: 1972, Rev. Geophys. Space Phys. 10, 837.

Munro, R. H., and Withbroe, G. L.: 1972, Astrophys. J. 176, 511.

Reber, E. E.: 1971, Solar Phys. 16, 75.

Shimabukuro, F. I.: 1968, Solar Phys. 5, 498.

Shimabukuro, F. I.: 1970, Solar Phys. 12, 438.

Shimabukuro, F. I., Chapman, G. A., Mayfield, E. B., and Edelson, S.: 1973, "On the Source of the Slowly Varying Component at Centimeter and Millimeter Wavelengths," ATR-73(8102)-8, The Aerospace Corp., El Segundo, Calif. (to appear in Solar Phys.)

Simon, P., and McIntosh, P. S.: 1972, in P. S. McIntosh and M. Dryer (eds.), Solar Activity Observations and Predictions (MIT Press, Cambridge, Mass.), p. 343.

Smith, Jr., J. B.: 1972, in P. S. McIntosh and M. Dryer (eds.), Solar Activity Observations and Predictions (MIT Press, Cambridge, Mass.) p. 429.

Syrovatskii, S. I.: 1966, Sov. Astron. AJ 10, 270.

Thomas, R. J., and Teske, R. G.: 1971, Solar Phys. 16, 431.

Waldmeier, M.: 1968-1973, "Heliographic Maps of the Photosphere for the Years 1967-1972" in Publikationen der Eidgenössichen Sternwarte Zürich, Schultess and Co., Zürich.

White, III, K. P.: 1972, "Solar Flare Forecasts Based on mm-Wavelength Measurements," ATR-73(8102)-4, The Aerospace Corp., El Segundo, Calif.

GLOSSARY

Active region:	A region on the sun characterized by stronger magnetic fields. Depending upon the field strength, an active region may exhibit some or all of the following: photospheric faculae; chromospheric plage; sunspots; filaments; a variety of associated coronal structures. These features constitute the active region, where solar flares are most likely to occur.
Center of activity:	Alternate terminology for an active region, but emphasizing more the characteristic association of flares and mass motions with active regions.
Class 1N flare:	An example of an importance classification for solar flares. The number indicates flare area from subflare to classes 1-4. The letter indicates flare brightness from faint (F) to normal (N) to bright (B).
Coronal hole:	A rather extensive region in the corona characterized by very low electron density, lower temperature, and general absence of any active regions; discovered in extreme-ultraviolet observations.
Faculae:	Bright points in a network surrounding sunspots, observable in the continuous (white-light) radiation. Faculae are a photospheric manifestation due to the presence of magnetic fields around sunspots.
Filament:	A linear, threadlike dark feature visible on the solar disk in the light of Hα. Filaments are intimately connected with magnetic fields. On the solar limb, a filament seen in profile is termed a prominence.

Filament Channel:	A pattern of very fine, linear structures, visible in the light of Hα, aligned to form a natural extension of, or replacement for, a filament.
Flare:	An explosive, short-lived (minutes to a couple hours) increased brightness emanating from a local region in the chromosphere, corona, and, sometimes, the photosphere. Flares have now been observed in x-rays, UV, visible light, radio wavelengths and energetic particles.
Hα(H-alpha):	The first spectrum line of the Balmer series of hydrogen at 6563Å. Observations in this line reveal the chromosphere and serve as the most widespread "atlas" of a host of chromospheric phenomena.
Longitudinal magnetic field:	The component of the magnetic field strength in the line of sight of the observer, in distinction to the transverse component. The longitudinal component is most easily and commonly measured at solar observatories.
McMath plage region:	A plage region which has been identified and assigned a number in a sequence established originally at the McMath-Hulbert Observatory.
Neutral line:	In reference to the longitudinal magnetic field, a dividing line between areas of opposite magnetic polarity.
Peak temperature enhancement:	The highest temperature enhancement reading at 3.3 mm in an active region, uninterpolated and unextrapolated.
Plage:	A network of bright points surrounding or in the vicinity of sunspot magnetic fields. Plage usually refers to the chromospheric manifestation, while faculae are the photospheric plage.

Plage corridor:	The separation between two distinct areas of plage, usually indicative of a magnetic polarity reversal.
Slowly varying component:	The component of radio emission, associated with sunspots, which varies in phase with sunspots, therefore showing a 27-day modulation due to solar rotation.
Solar disk:	The visible "face" of the sun, as distinct from the solar limb.
Temperature enhancement:	The term employed to represent the excess temperature measured at 3.3 mm for active regions as referenced to a quiet, normalization point.

Figure Captions

Fig. 1 The flare-record chart covering the period 1 June 1970 to 15 May 1973. All plage regions producing flares of class $\geq$ 1B qualify to be on the chart and are represented by the triangle symbols, whose vertices indicate the day and decimal of a day of central meridian crossing. The McMath plage numbers from 10780 to 12336 are indicated, as well as the latitudes of the plage centers and the NOAA regional flare indices (inside the triangles). The plage regions identified as belonging to a recurrent family of flare-prone regions are indicated by blackened vertices. Preliminary data for the most recent period are indicated by small squares.

Fig. 2 For Carrington rotation 1516, the synoptic 3.3-mm radio map has been superimposed on the corresponding heliographic map of the sun by Waldmeier (1968). Note the close correspondence between the 4% contour levels and facular areas and between the peak enhancements and sunspots.

Fig. 3 Same as Fig. 2, but for rotation 1518.

Fig. 4 Same as Fig. 2, but for rotation 1521.

Fig. 5 Same as Fig. 2, but for rotation 1530.

Fig. 6 Same as Fig. 2, but for rotation 1531.

Fig. 7 For Carrington rotation 1523, the synoptic 3.3-mm radio map is compared with the corresponding Hα-synoptic map, courtesy of P. S. McIntosh (NOAA-Boulder).

Legend: filaments are cross-hatched; Hα plages are stippled; plage corridors are lines through stippled areas; filament channels are solid lines outside active regions; sunspots are large dots; and dashed lines are estimates/interpolations of filament channels.

Fig. 8 Same as Fig. 7, but for rotation 1524.

Fig. 9 Data taken from White (1972) showing the probability of occurrence of a class 1N flare from a flare-prone plage region as a function of the daily measured peak temperature enhancement. The forecast probability is valid for a one to two day period following the radio map.

Page intentionally left blank

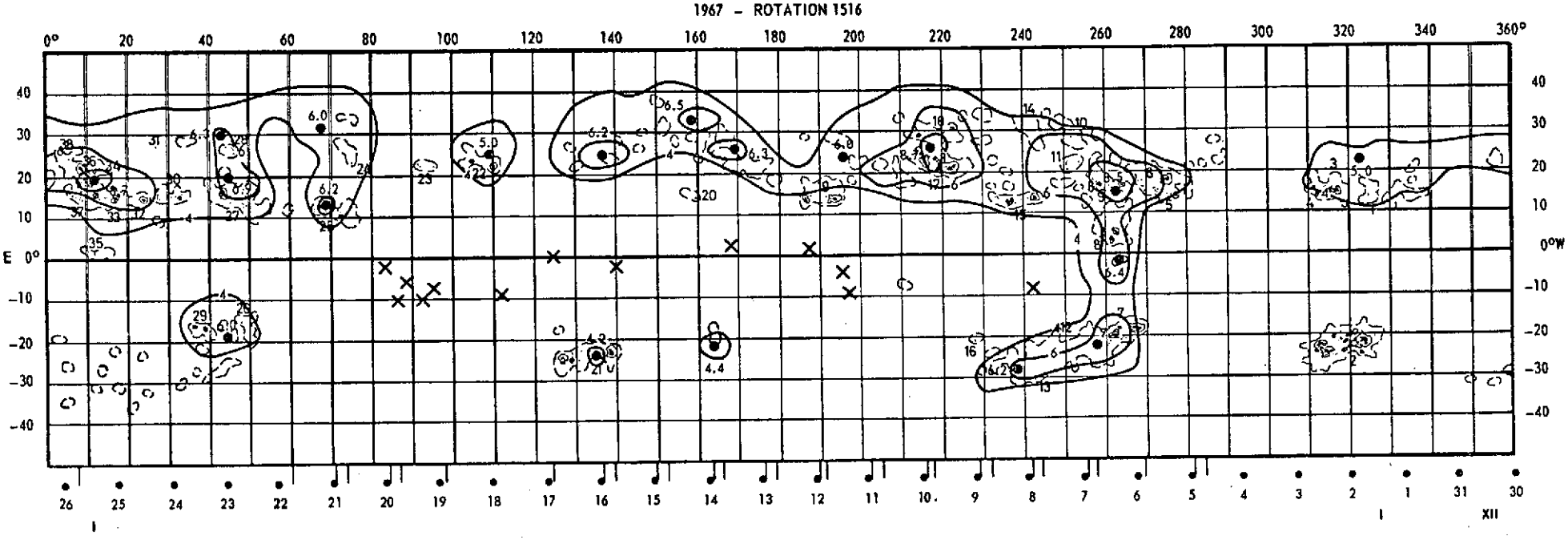
1967 - ROTATION 1516
0°
20
40
60
80
100
120
140
160
180
200
220
240
260
280
300
320
340
360°
40
30
20
10
E 0°
-10
-20
-30
-40
0°W
26
25
24
23
22
21
20
19
18
17
16
15
14
13
12
11
10
9
8
7
6
5
4
3
2
1
31
30
I
XII

Fig. 2

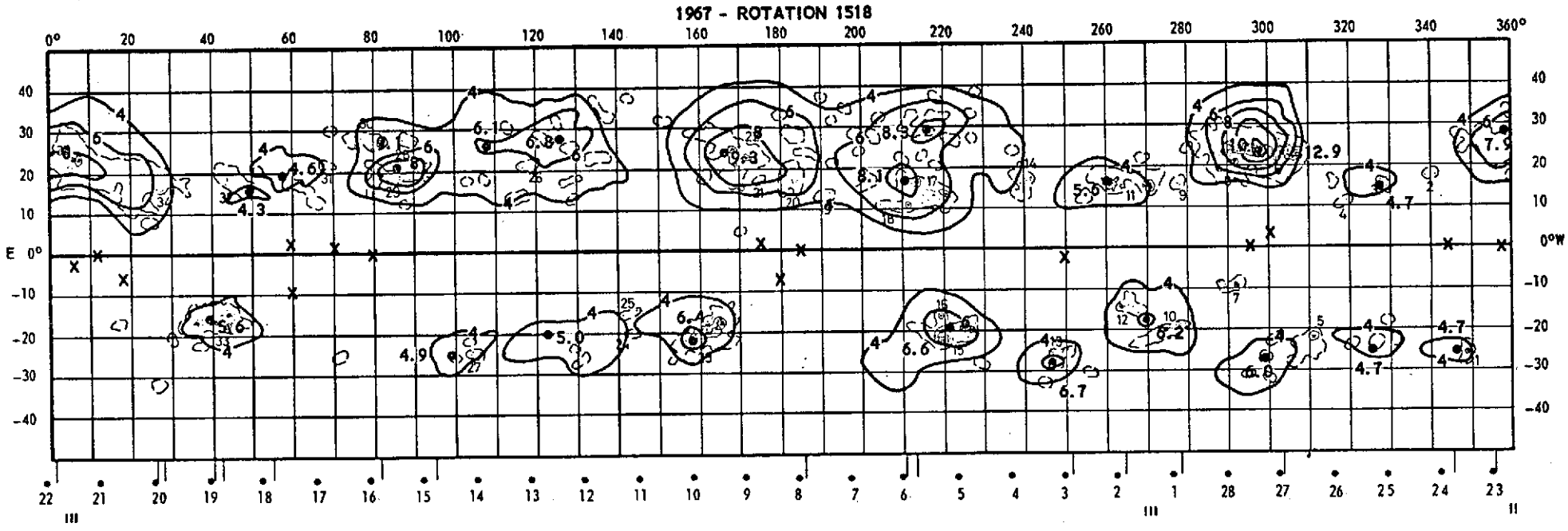
1967 - ROTATION 1518
0° 20 40 60 80 100 120 140 160 180 200 220 240 260 280 300 320 340 360°
40 30 20 10 E 0° -10 -20 -30 -40
40 30 20 10 0°W -10 -20 -30 -40
22 21 20 19 18 17 16 15 14 13 12 11 10 9 8 7 6 5 4 3 2 1 28 27 26 25 24 23
III
III
II

Fig. 3

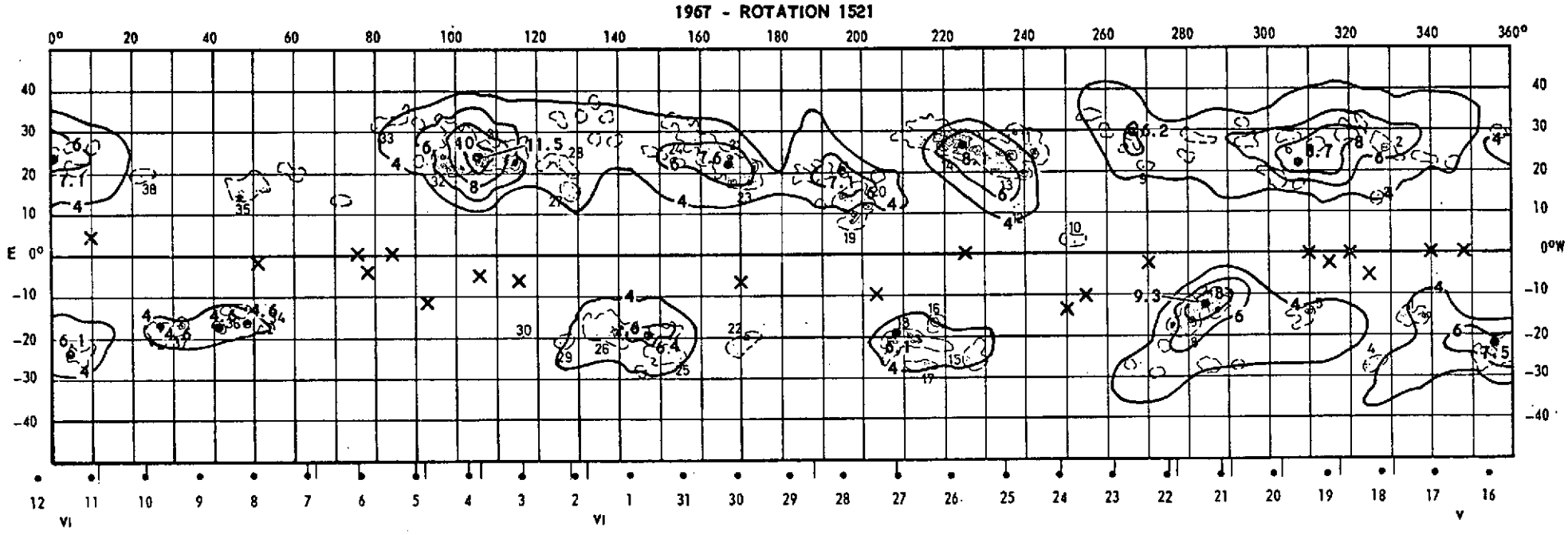
1967 - ROTATION 1521
0° 20 40 60 80 100 120 140 160 180 200 220 240 260 280 300 320 340 360°
40 30 20 10 E 0° -10 -20 -30 -40
0°W
12 11 10 9 8 7 6 5 4 3 2 1 31 30 29 28 27 26 25 24 23 22 21 20 19 18 17 16
VI VI V

Fig. 4

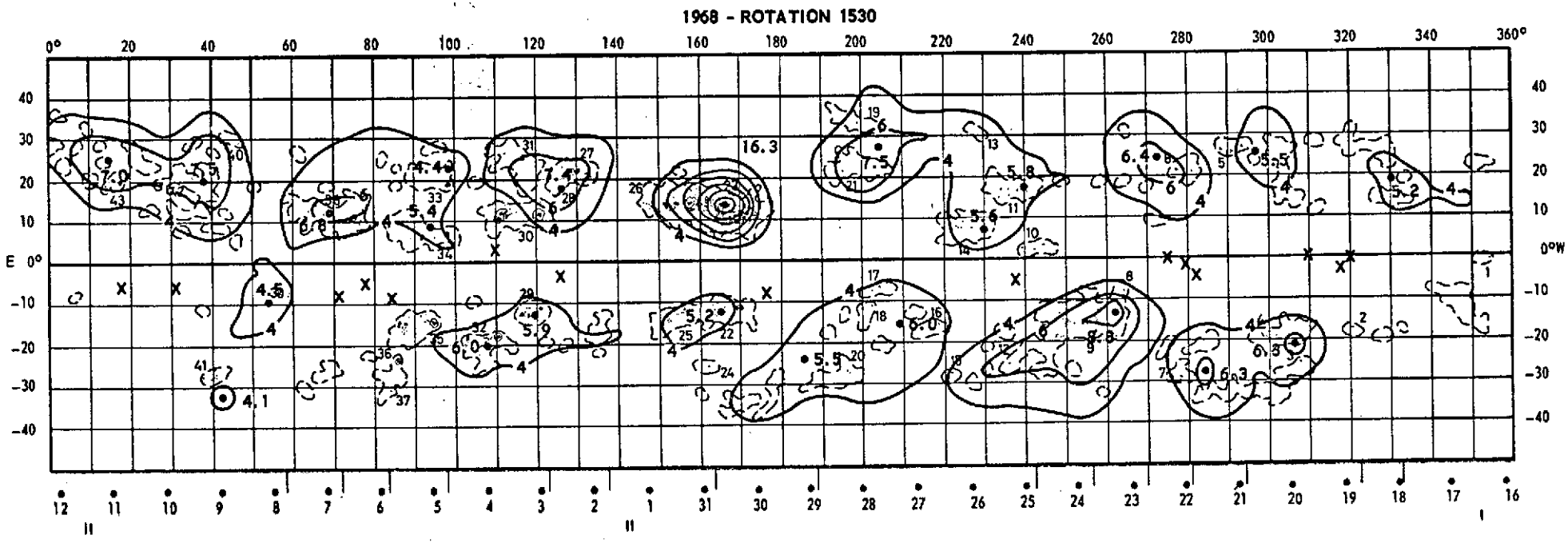
1968 - ROTATION 1530
0° 20 40 60 80 100 120 140 160 180 200 220 240 260 280 300 320 340 360°
40 30 20 10 E 0° -10 -20 -30 -40
40 30 20 10 0°W -10 -20 -30 -40
16.3
12 11 10 9 8 7 6 5 4 3 2 1 31 30 29 28 27 26 25 24 23 22 21 20 19 18 17 16
II II I

Fig. 5

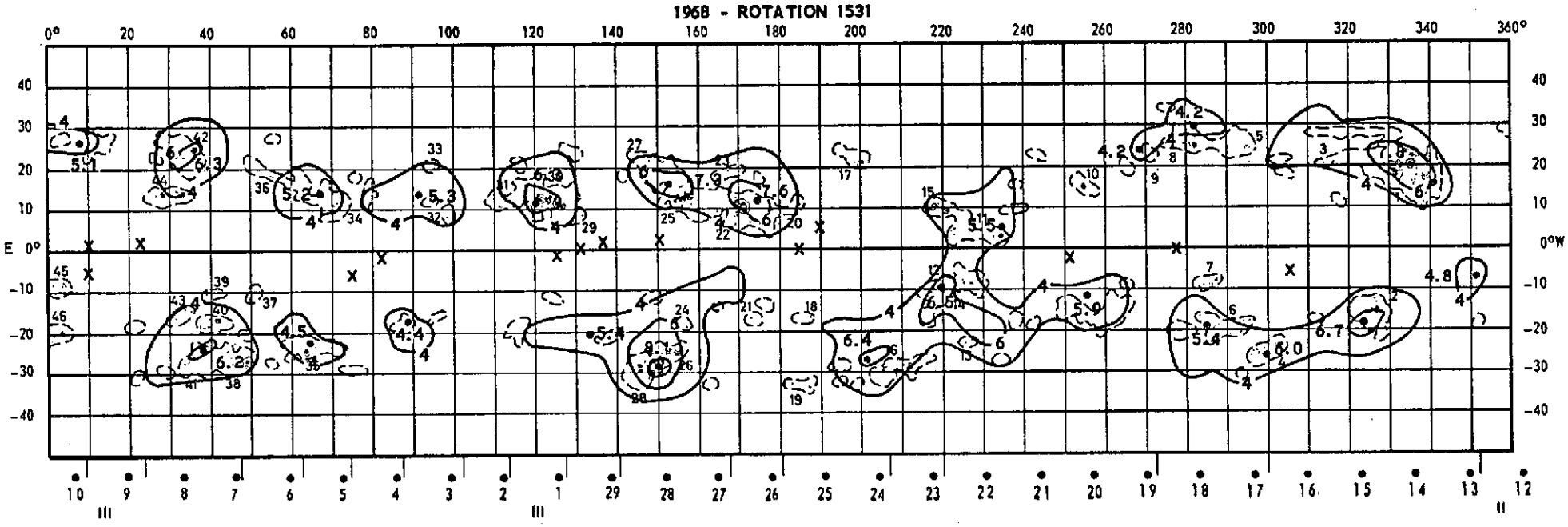
1968 - ROTATION 1531
0° 20 40 60 80 100 120 140 160 180 200 220 240 260 280 300 320 340 360°
40 30 20 10 E 0° -10 -20 -30 -40
0°W
10 9 8 7 6 5 4 3 2 1 29 28 27 26 25 24 23 22 21 20 19 18 17 16 15 14 13 12
III III II

Fig. 6

Fig. 7

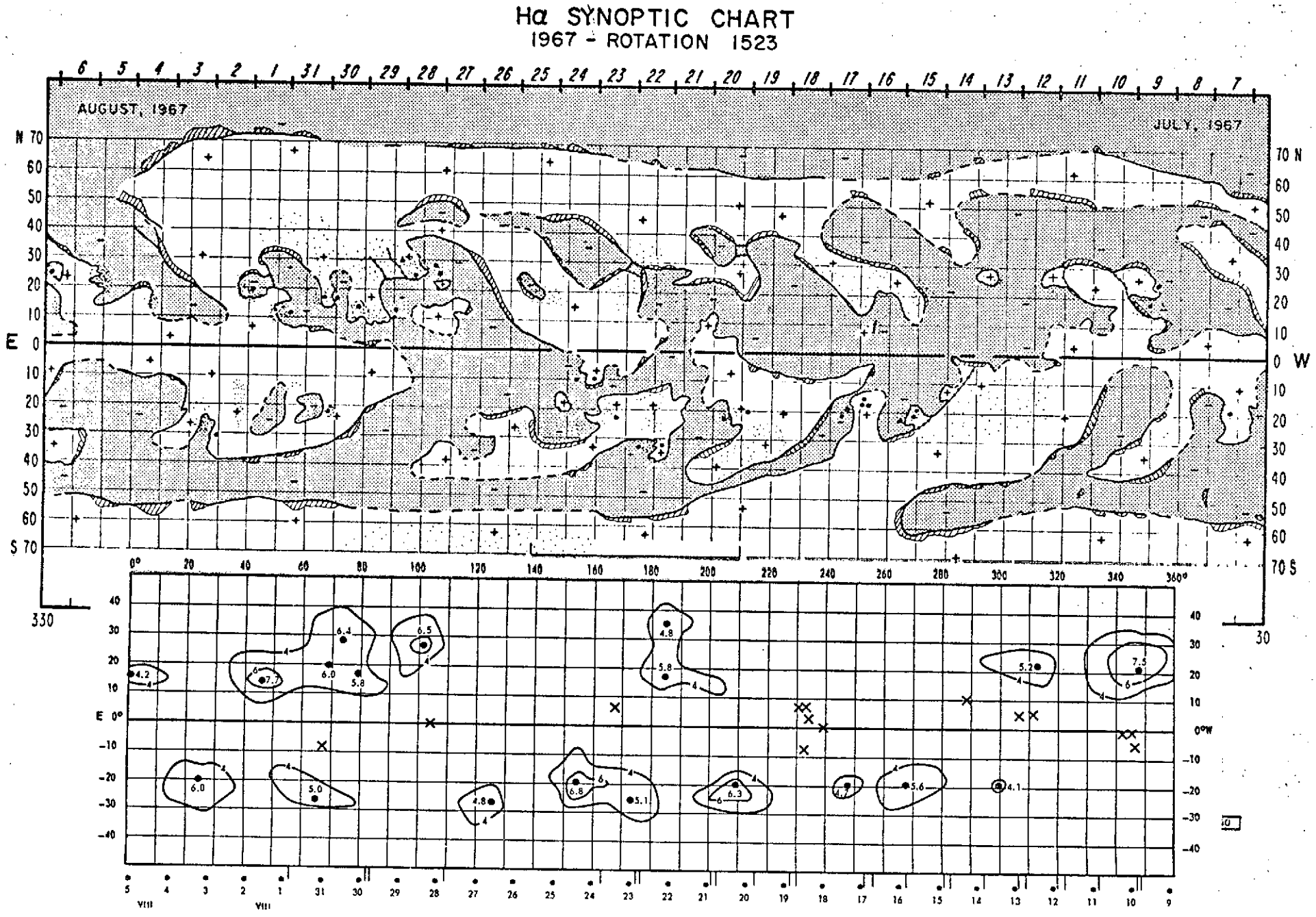
Hα SYNOPTIC CHART
1967 - ROTATION 1523
AUGUST, 1967
JULY, 1967
N 70
S 70
E
W
70 N
70 S
330
30

Fig. 8

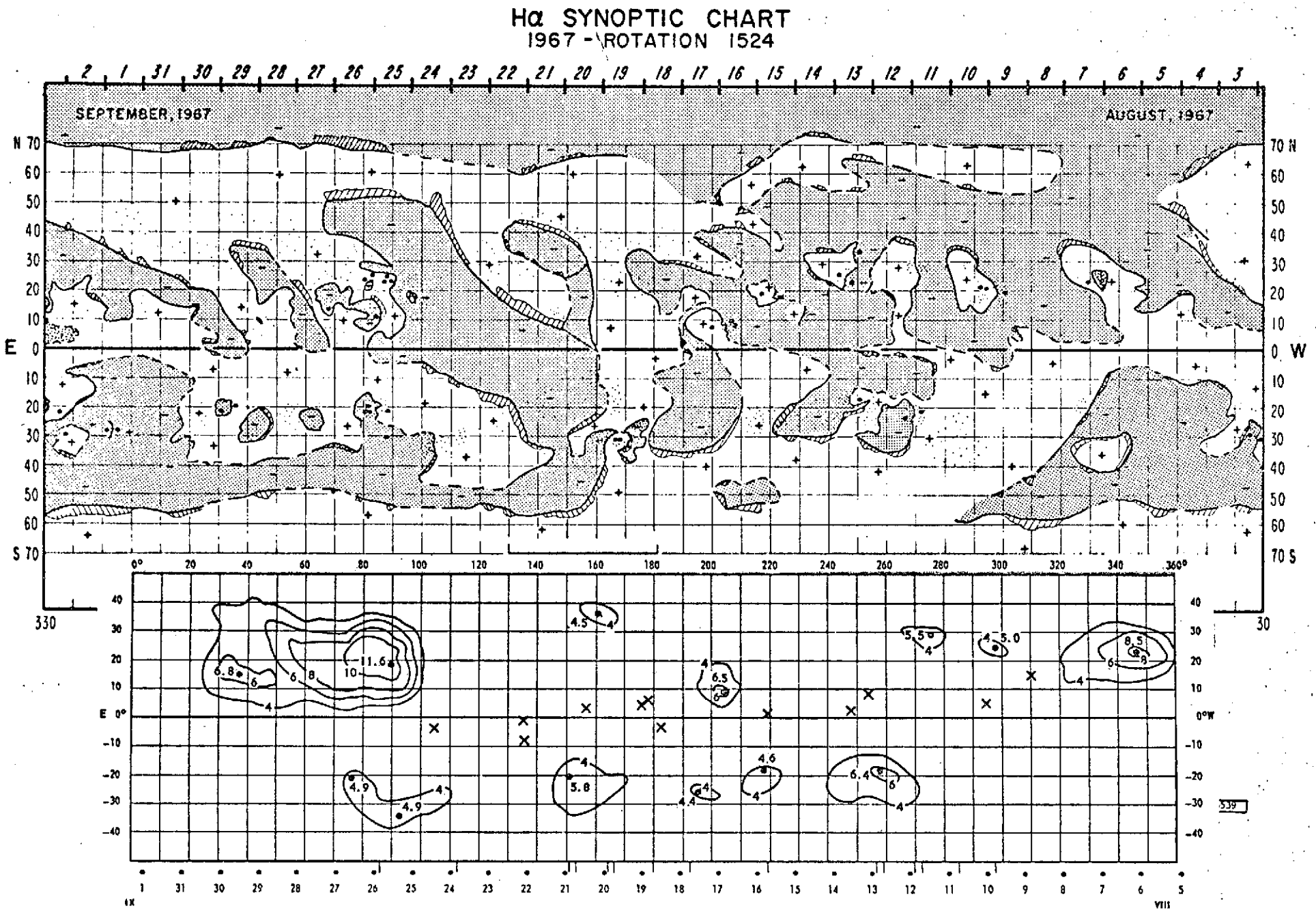
Hα SYNOPTIC CHART
1967 - ROTATION 1524
SEPTEMBER, 1967
AUGUST, 1967
2 1 31 30 29 28 27 26 25 24 23 22 21 20 19 18 17 16 15 14 13 12 11 10 9 8 7 6 5 4 3
N 70 60 50 40 30 20 10 E 0 10 20 30 40 50 60 S 70
70 N 60 50 40 30 20 10 0 W 10 20 30 40 50 60 70 S
0° 20 40 60 80 100 120 140 160 180 200 220 240 260 280 300 320 340 360°
330
30
E 0°
0°W
539
1 31 30 29 28 27 26 25 24 23 22 21 20 19 18 17 16 15 14 13 12 11 10 9 8 7 6 5
IX
VIII

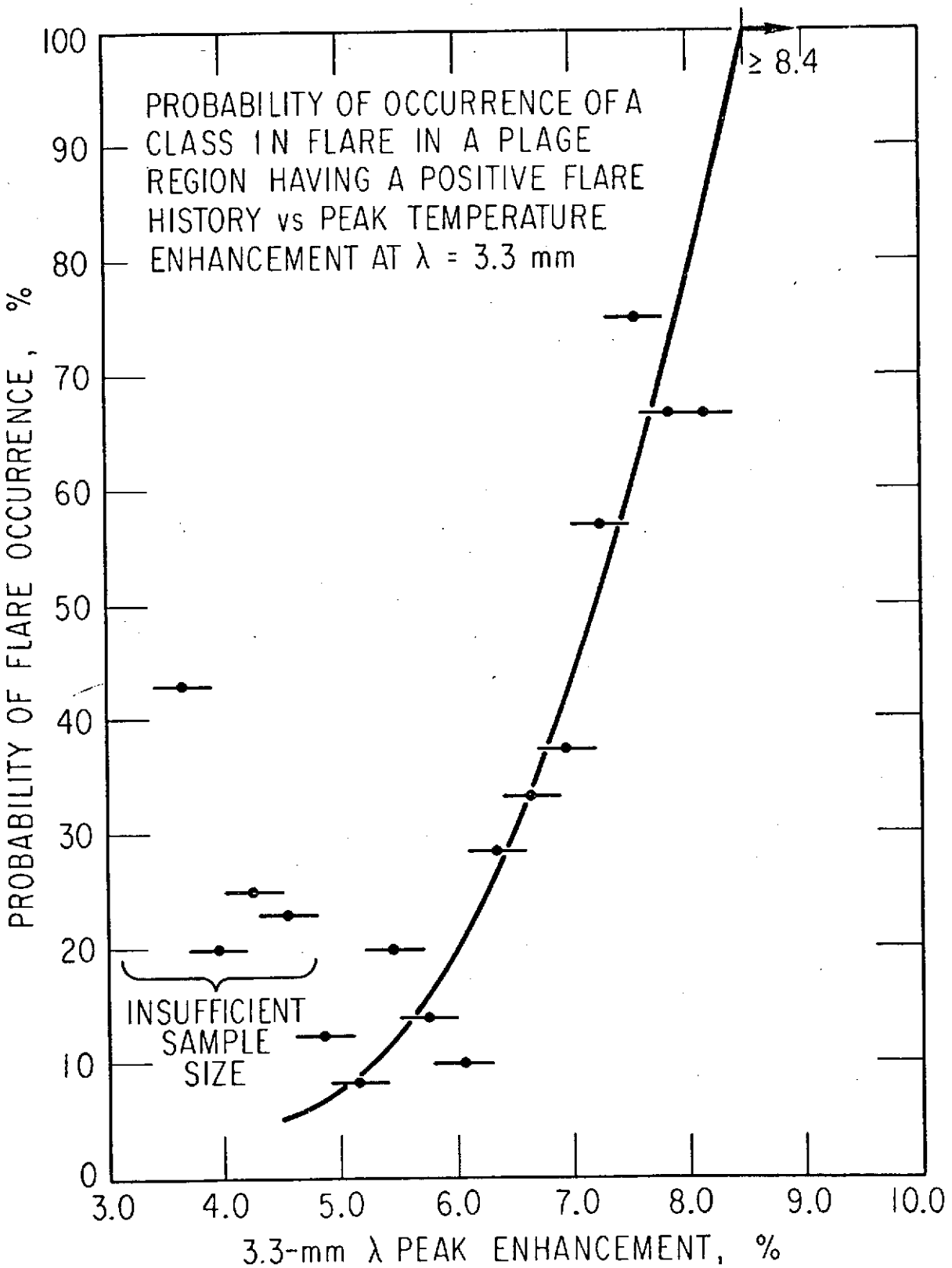
PROBABILITY OF OCCURRENCE OF A CLASS 1 N FLARE IN A PLAGE REGION HAVING A POSITIVE FLARE HISTORY vs PEAK TEMPERATURE ENHANCEMENT AT λ = 3.3 mm
≥ 8.4
INSUFFICIENT SAMPLE SIZE
PROBABILITY OF FLARE OCCURRENCE, %
3.3-mm λ PEAK ENHANCEMENT, %
0
10
20
30
40
50
60
70
80
90
100
3.0
4.0
5.0
6.0
7.0
8.0
9.0
10.0

Fig. 9

Appendix A

Figures 10-21 Synoptic 3.3-mm radio maps covering Carrington rotations 1516-1539 (1967 and 1968) minus rotation 1525, for which there are no data available. The contours are at levels of 4, 6, 8%, etc., enhancement above the quiet regions indicated by crosses. Peak enhancements are also shown.

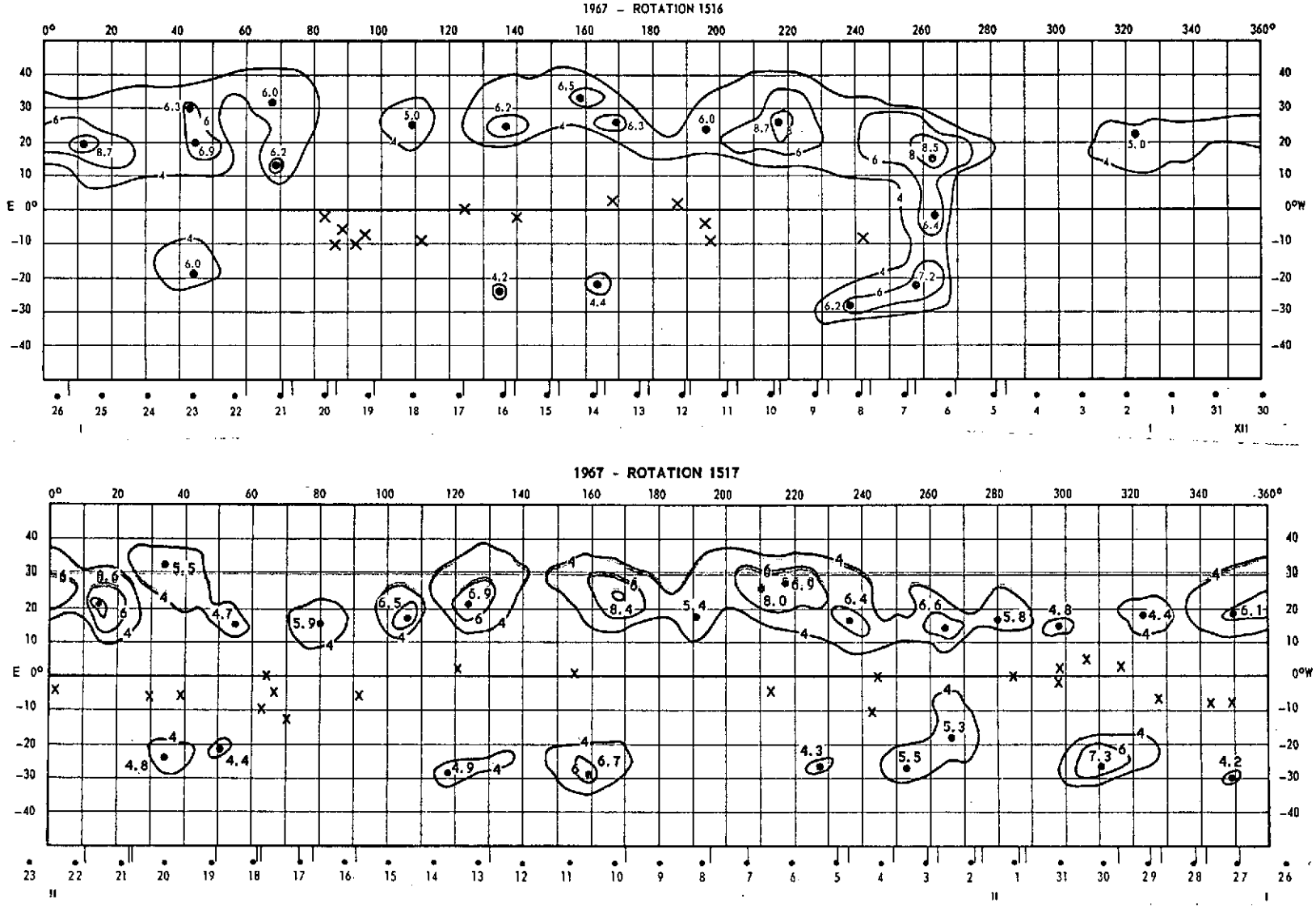

Fig. 10

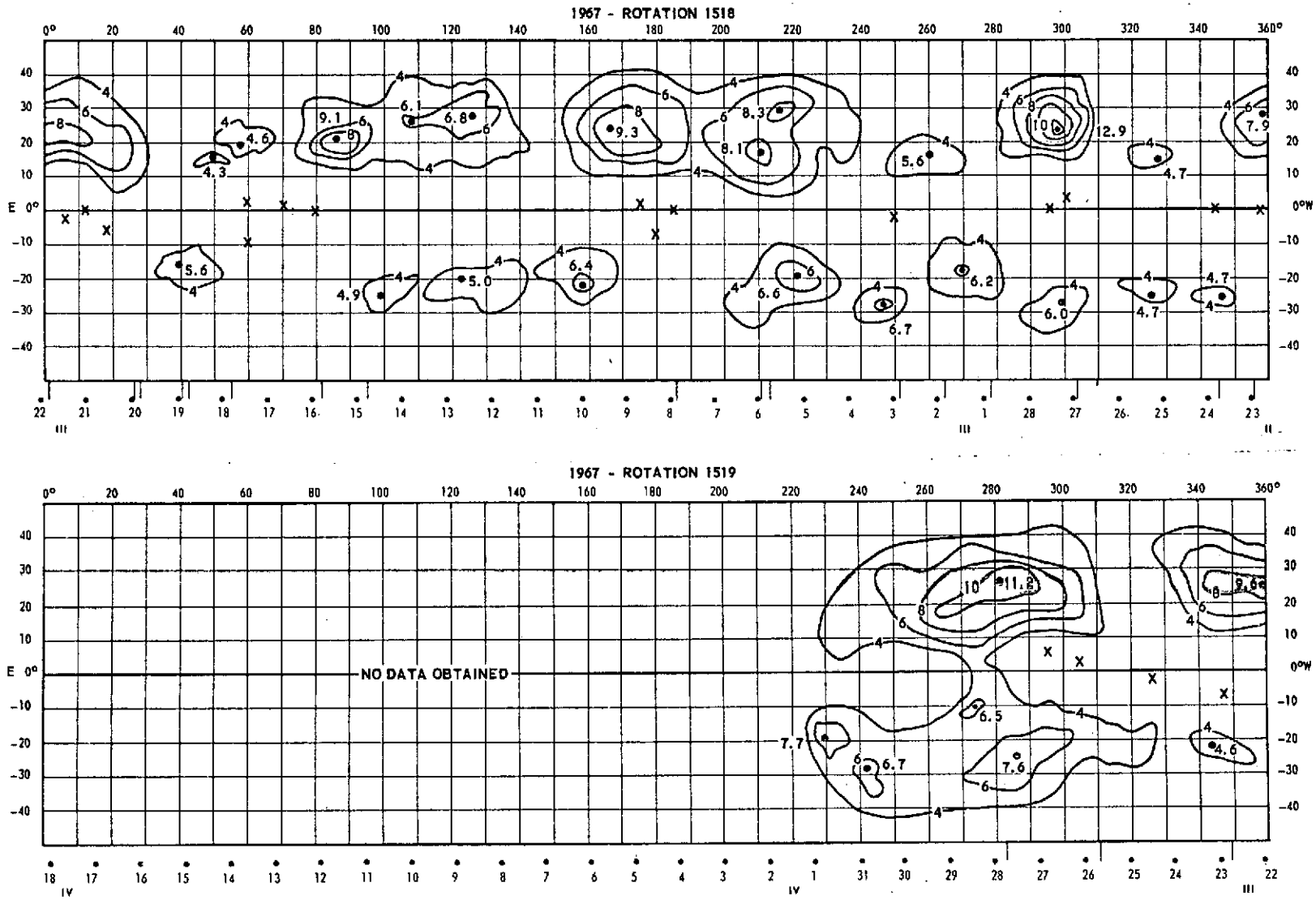

Fig. 11

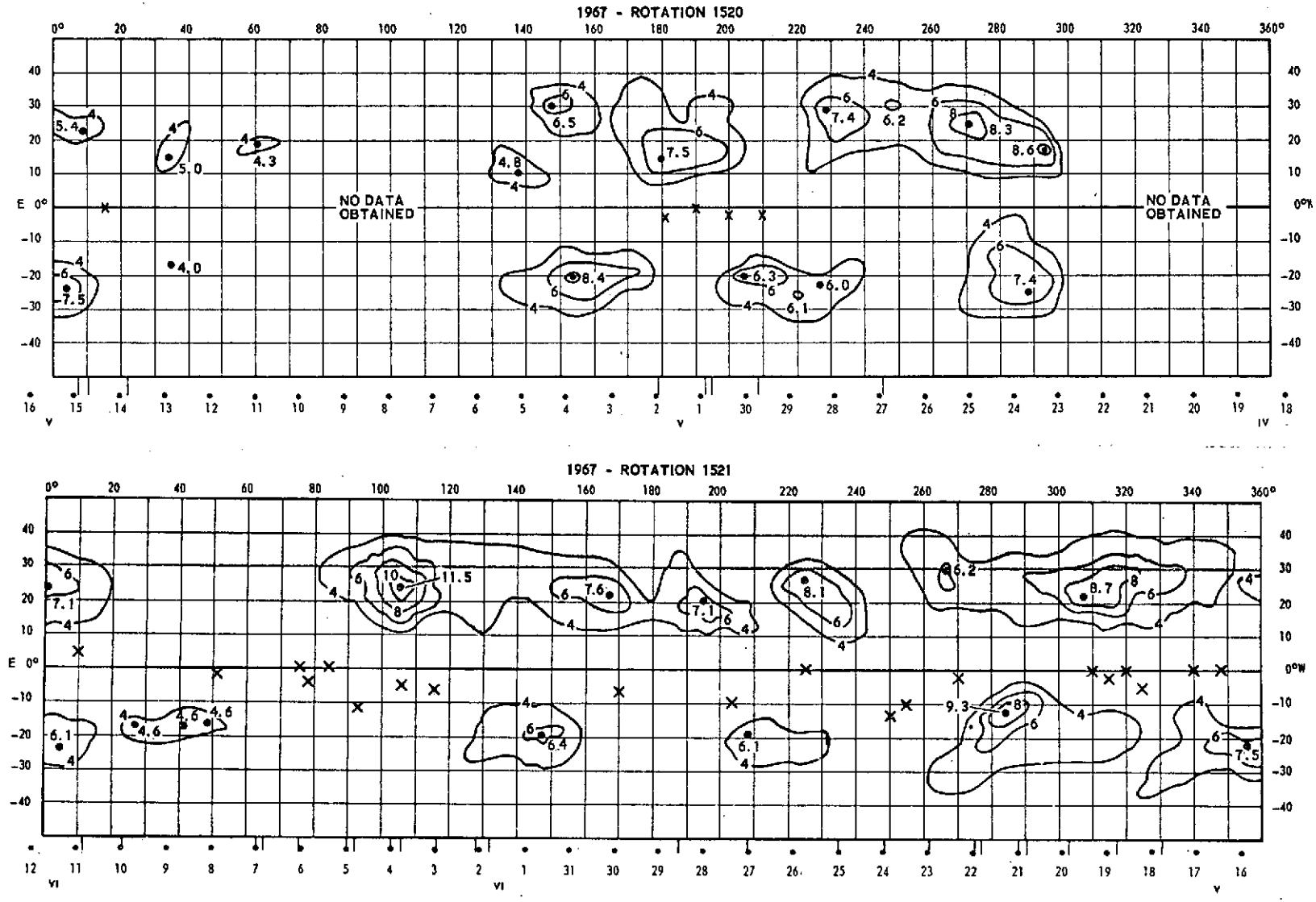
1967 - ROTATION 1520
NO DATA OBTAINED
NO DATA OBTAINED
1967 - ROTATION 1521

Fig. 12

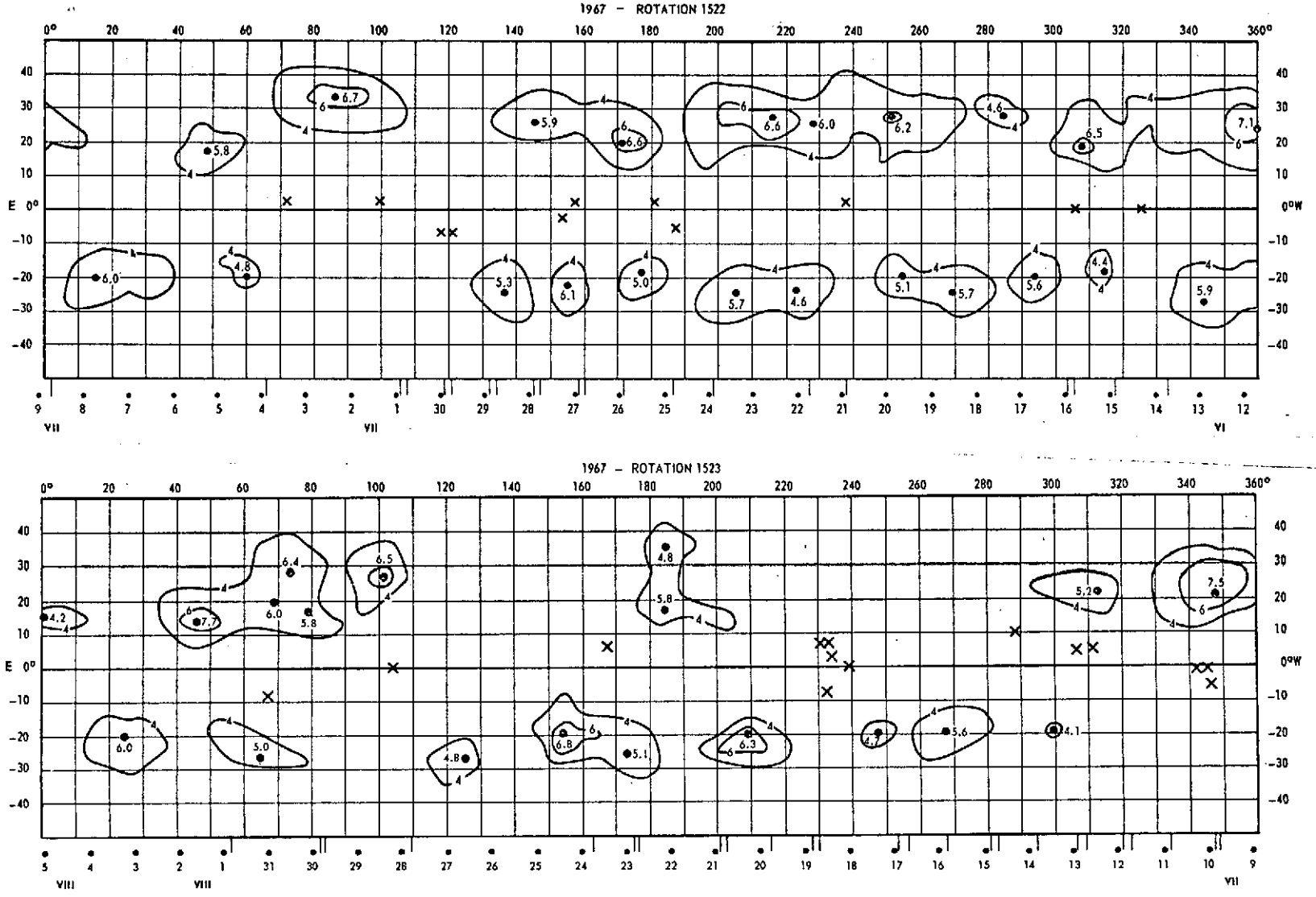

Fig. 13

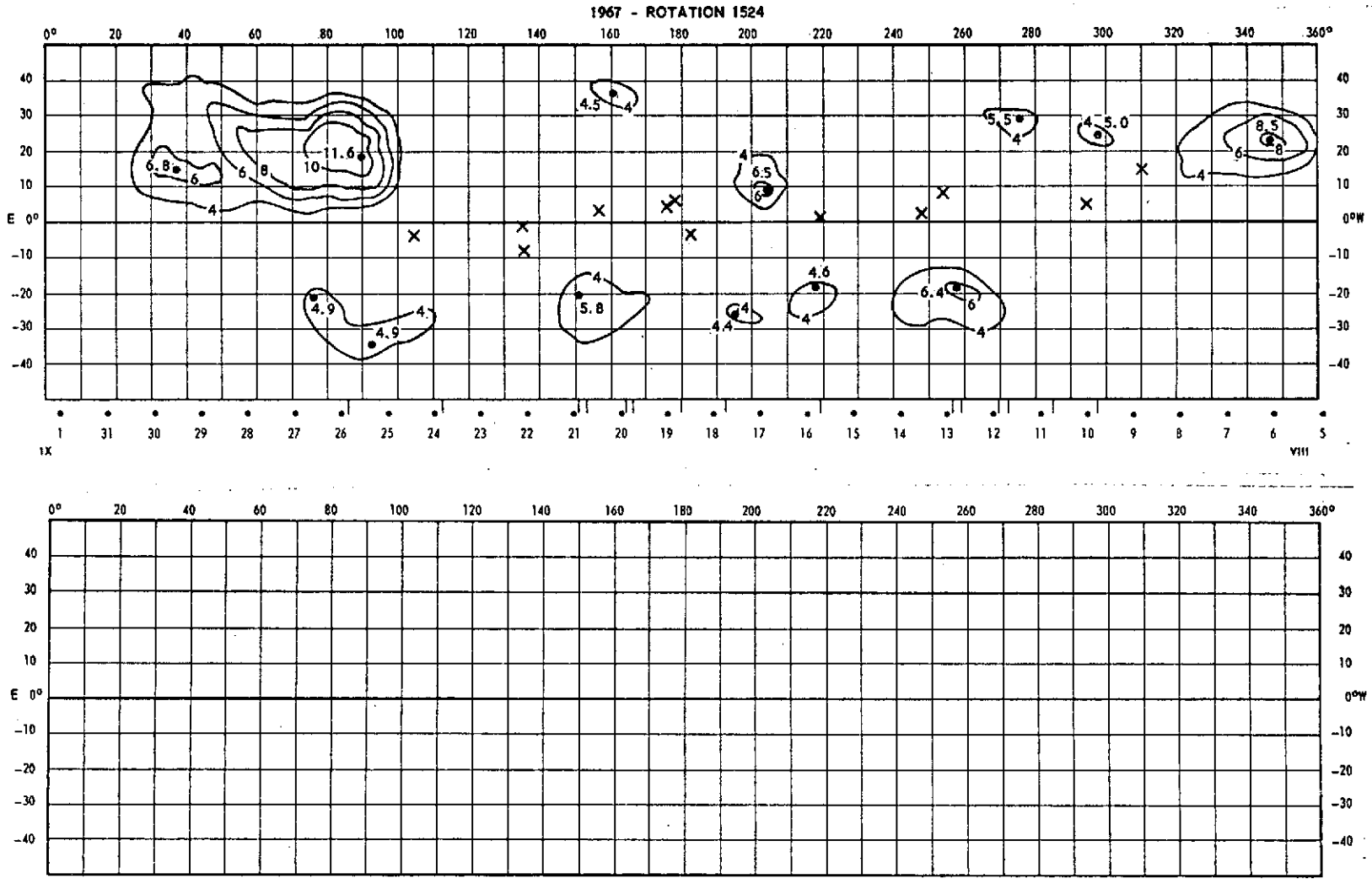
1967 - ROTATION 1524
0° 20 40 60 80 100 120 140 160 180 200 220 240 260 280 300 320 340 360°
40 30 20 10 E 0° −10 −20 −30 −40
0°W
1 31 30 29 28 27 26 25 24 23 22 21 20 19 18 17 16 15 14 13 12 11 10 9 8 7 6 5
IX
VIII
11.6
10
6.8
6
8
4.5
5.5
5.0
8.5
6.5
4.9
5.8
4.6
4.4
6.4

Fig. 14

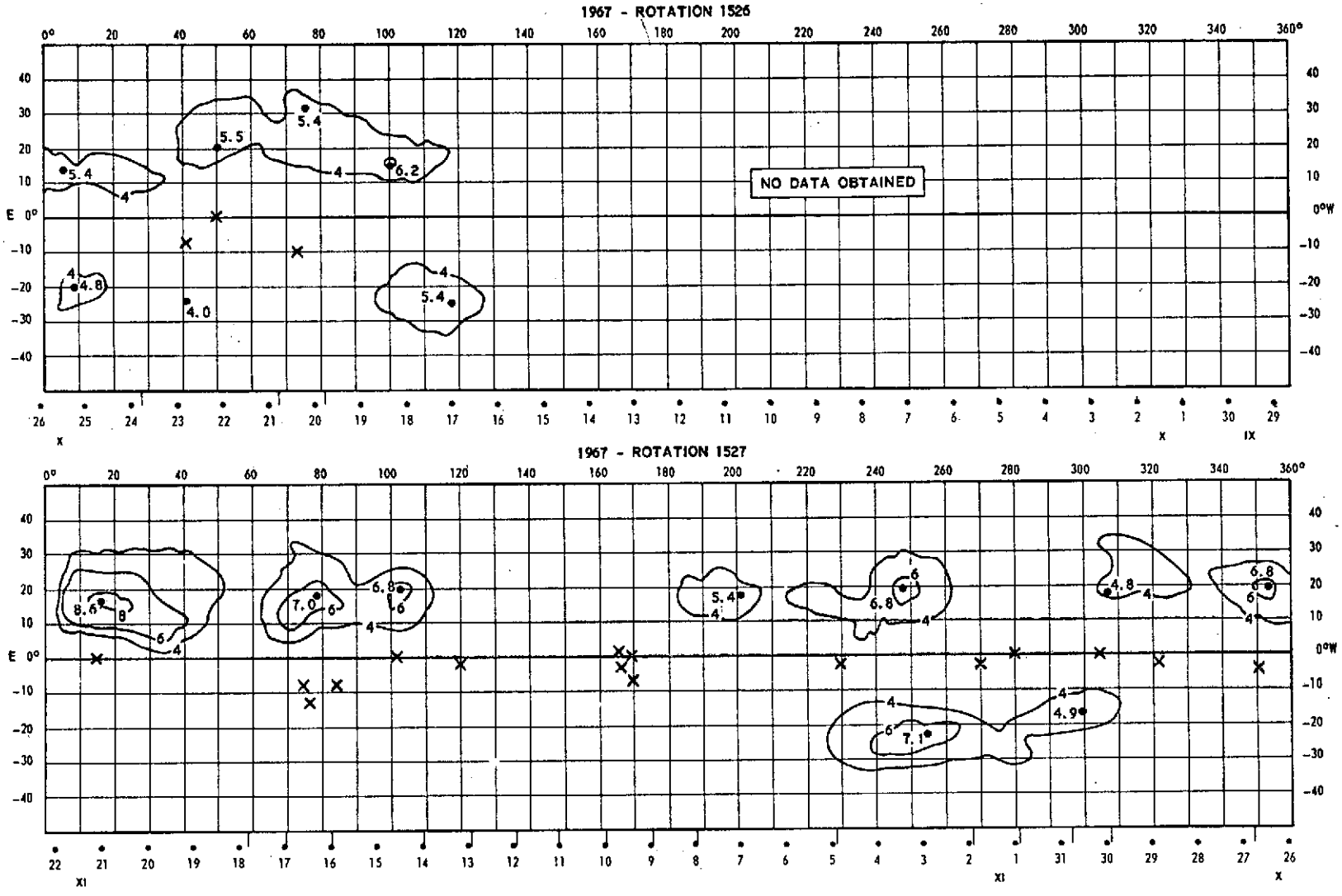

Fig. 15

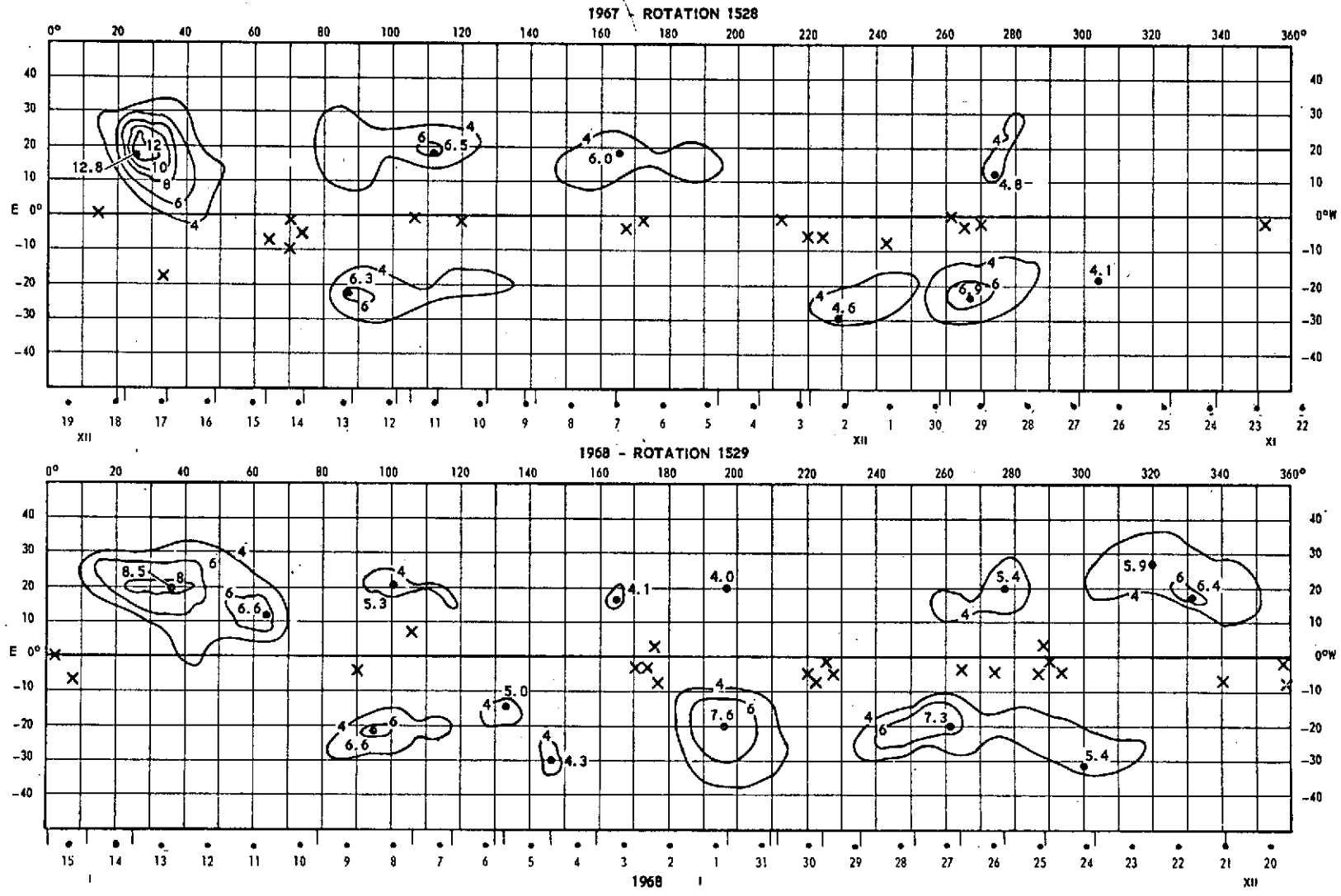

Fig. 16

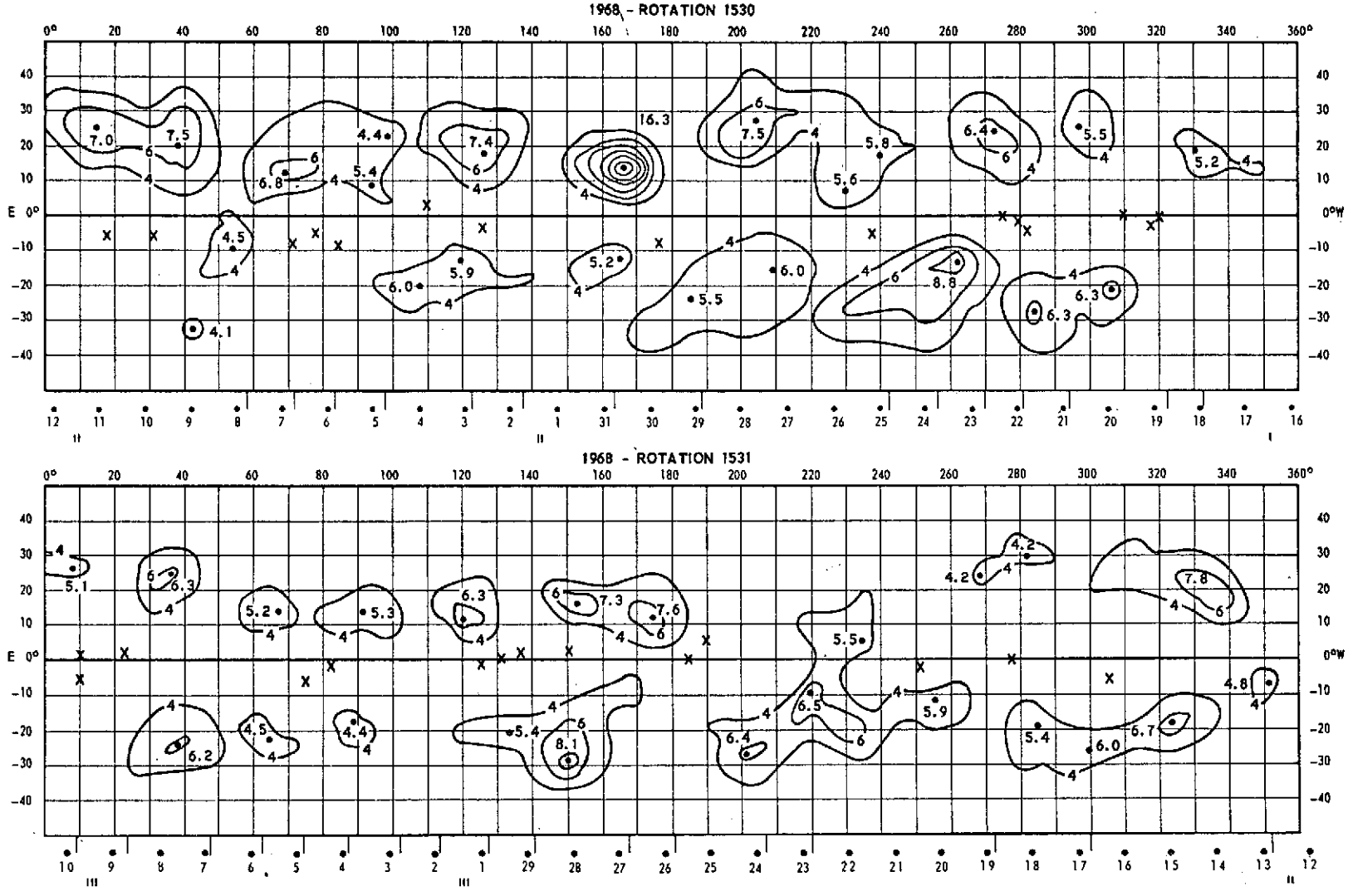

Fig. 17

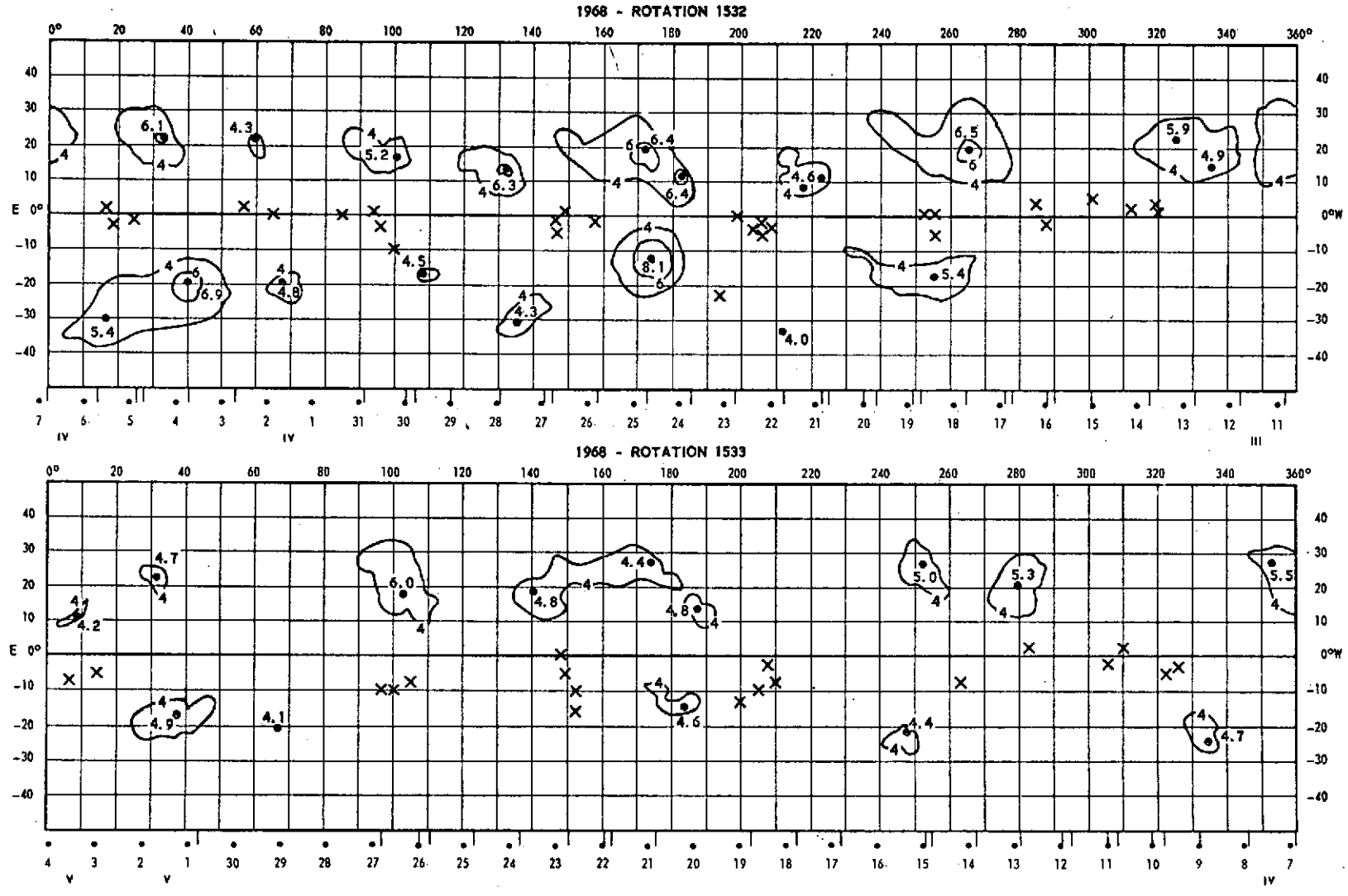

Fig. 18

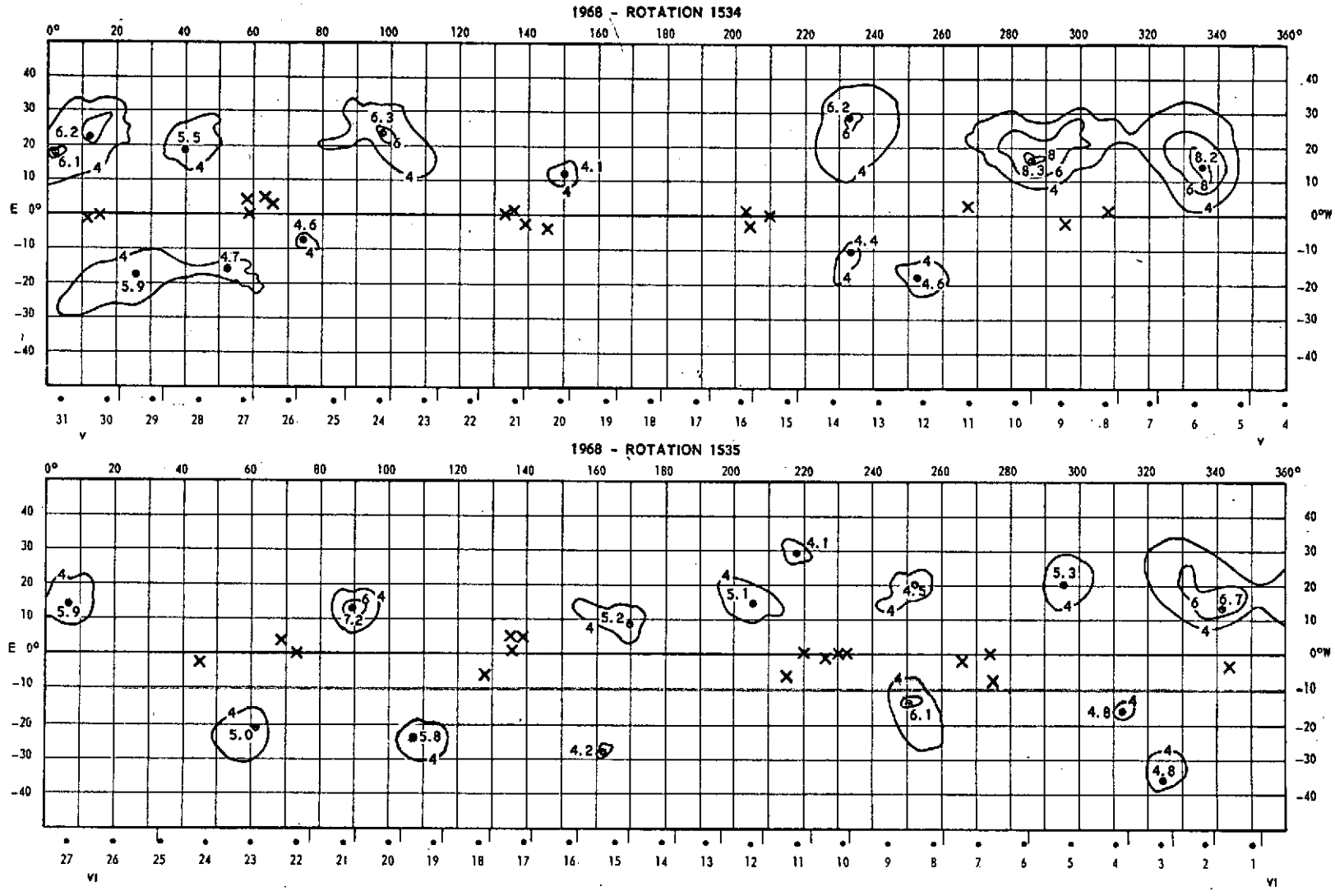

Fig. 19

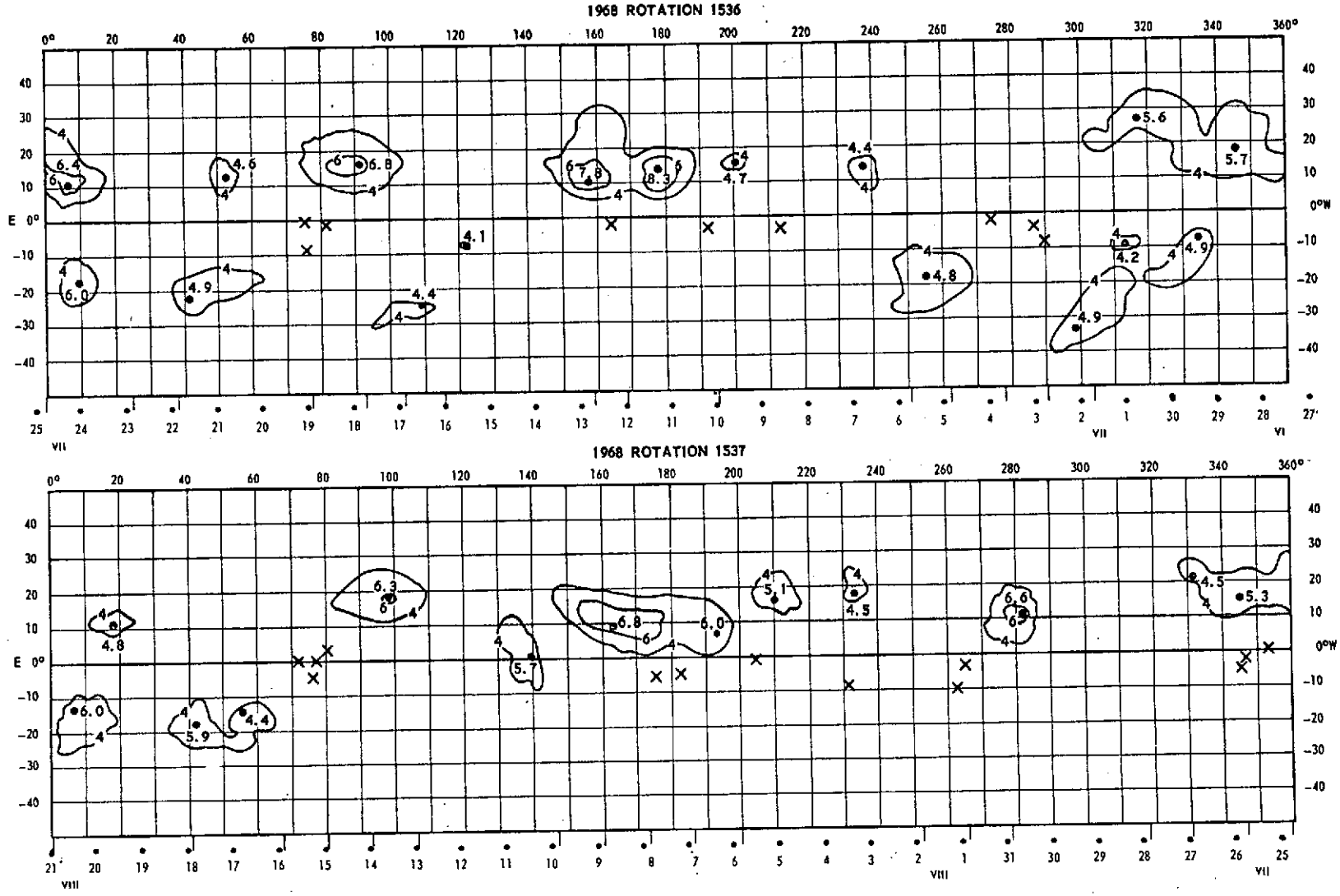

Fig. 20

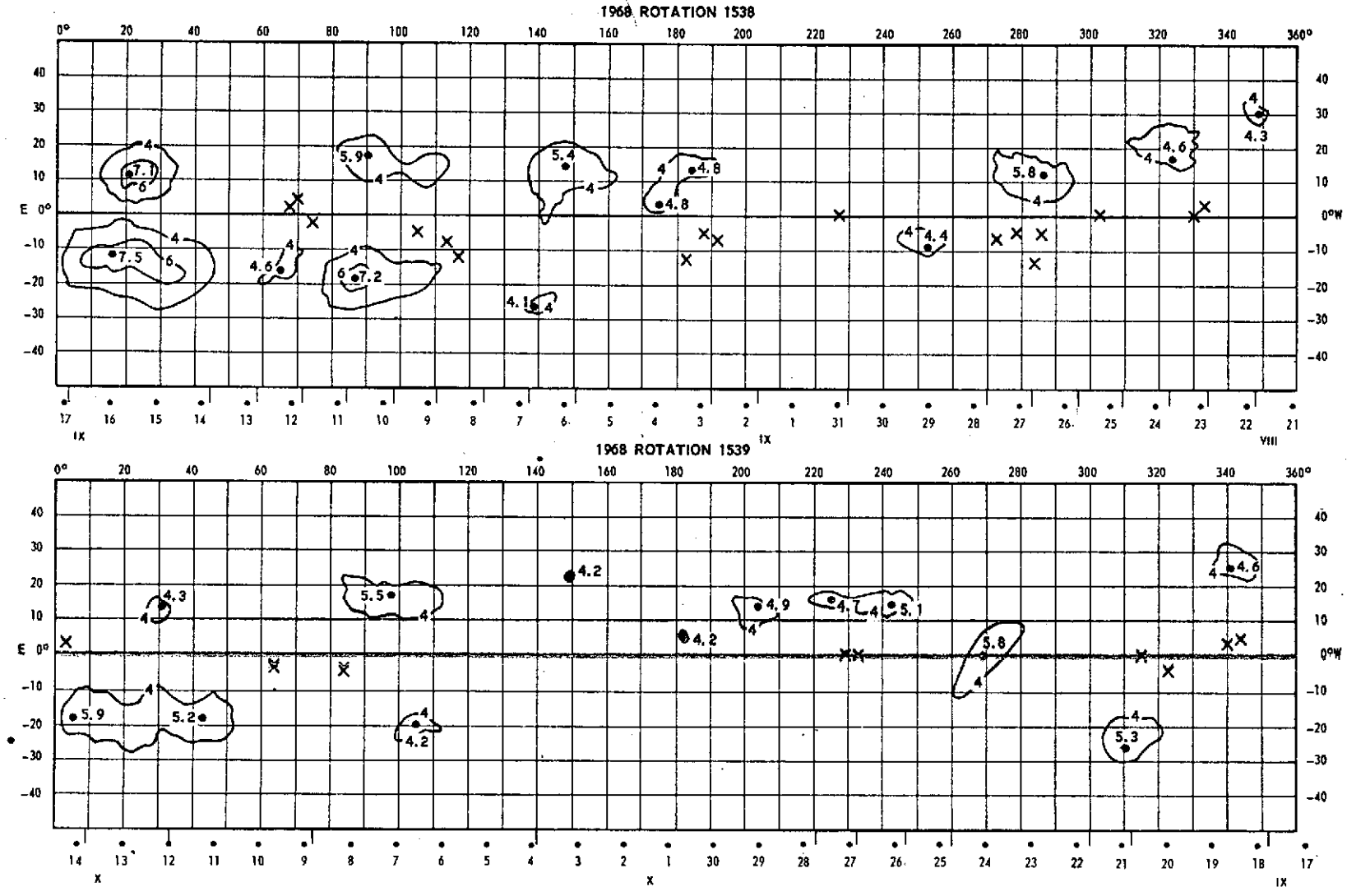
1968 ROTATION 1538
1968 ROTATION 1539
0°
20
40
60
80
100
120
140
160
180
200
220
240
260
280
300
320
340
360°
E 0°
0°W
IX
X
VIII

Fig. 21

Appendix B

Figures 22-33 Synoptic flare charts covering Carrington rotations 1516-1539 (1967 and 1968). Each center of activity is designated by a McMath calcium plage number, latitude, and Carrington longitude. Flare designations are as follows: importance class 1, open circle; 2, filled circle; 3, triangle; 4, square. The index number according to Dodson and Hedeman (1971) is given beside each flare.

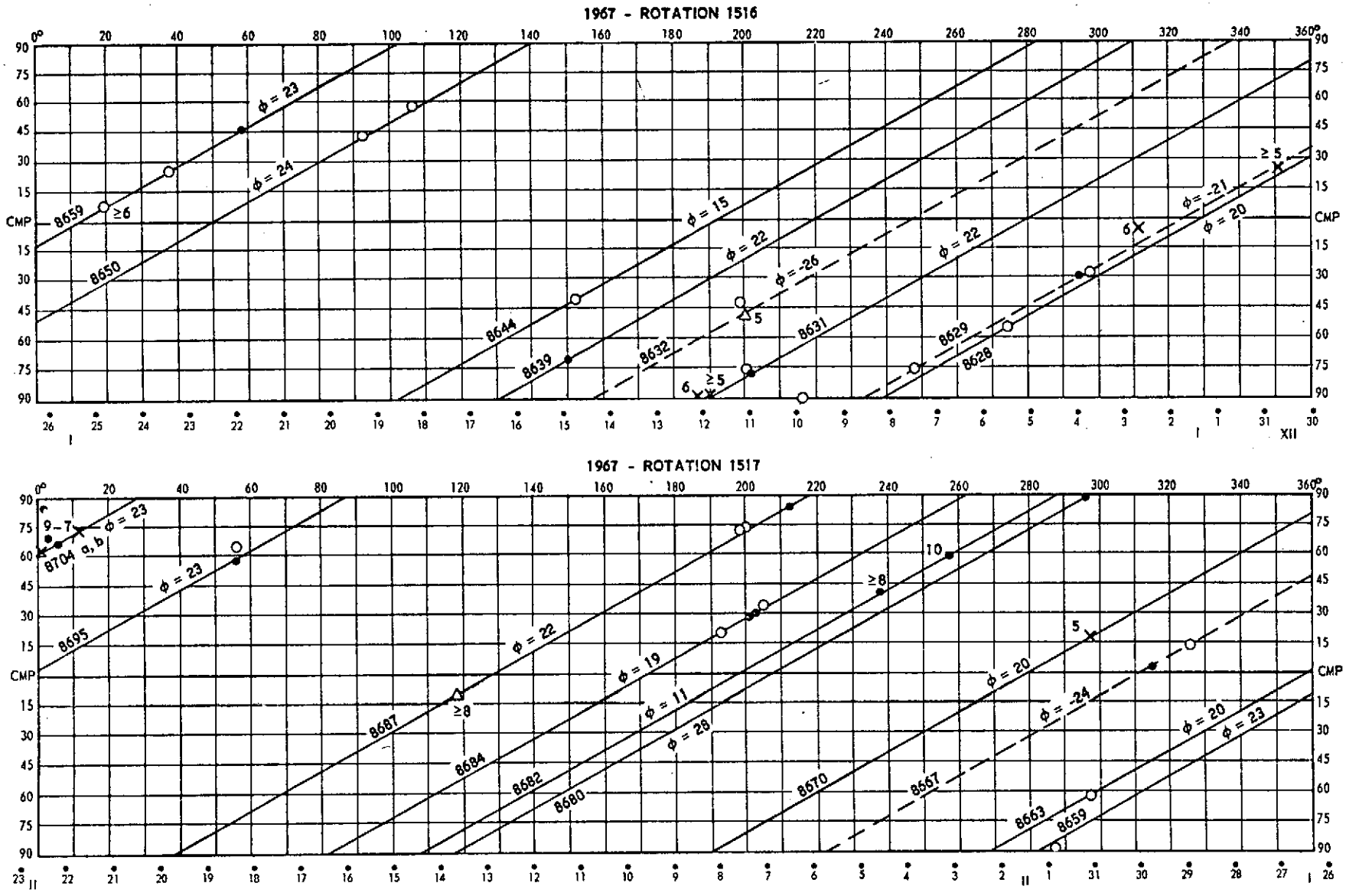
1967 - ROTATION 1516
CMP
8659
≥6
8650
ϕ = 23
ϕ = 24
8644
8639
ϕ = 15
ϕ = 22
ϕ = -26
5
8632
8631
6
≥5
ϕ = 22
8629
8628
6
ϕ = -21
ϕ = 20
≥5
1967 - ROTATION 1517
9-7
ϕ = 23
8704
a, b
ϕ = 23
8695
8687
≥8
ϕ = 22
8684
8682
8680
ϕ = 19
ϕ = 11
ϕ = 28
≥8
10
8670
5
ϕ = 20
8667
ϕ = -24
8663
8659
ϕ = 20
ϕ = 23

Fig. 22

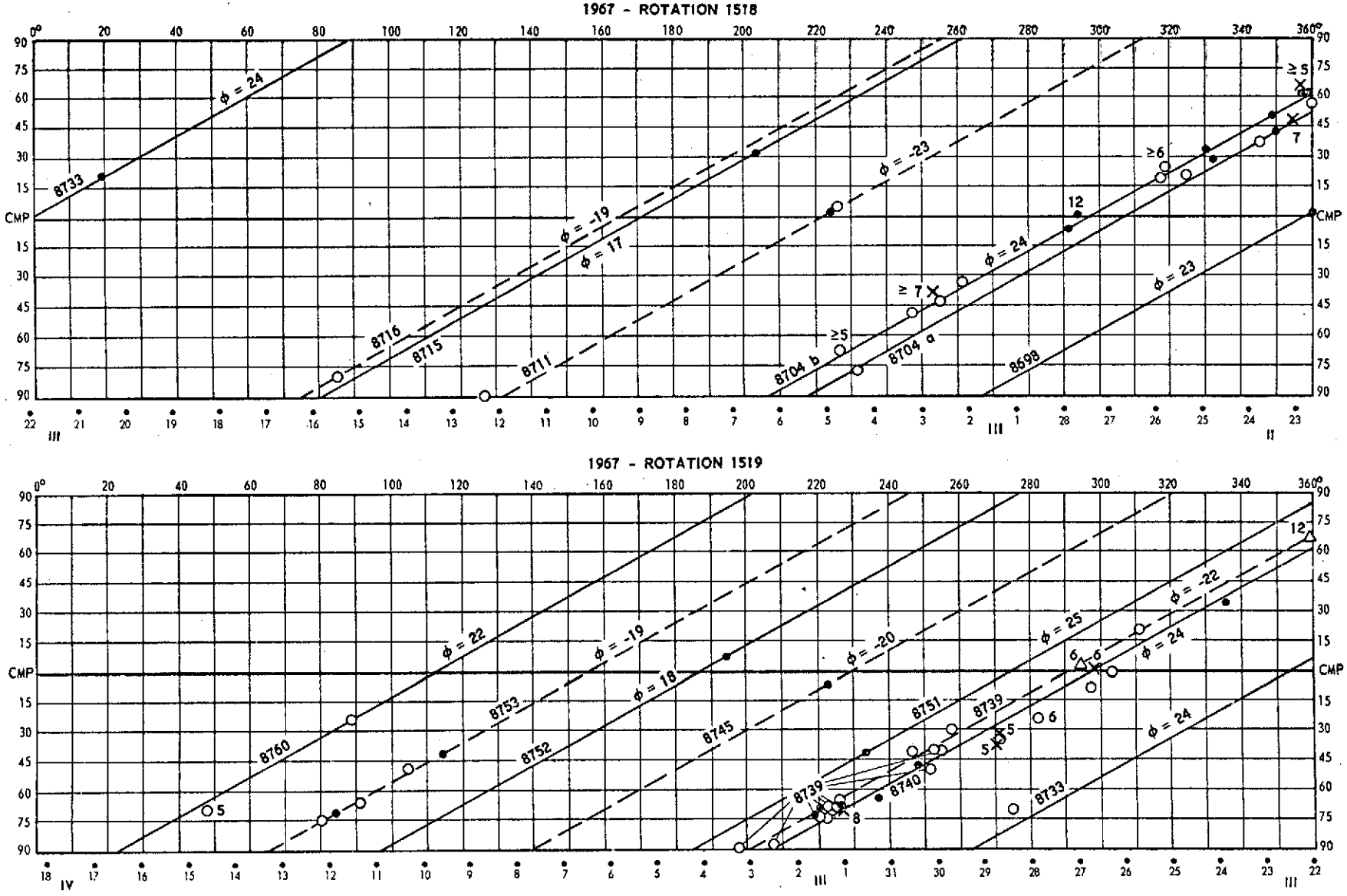
1967 - ROTATION 1518
1967 - ROTATION 1519
CMP
8733
8716
8715
8711
8704 b
8704 a
8698
8760
8753
8752
8745
8751
8739
8740

Fig. 23

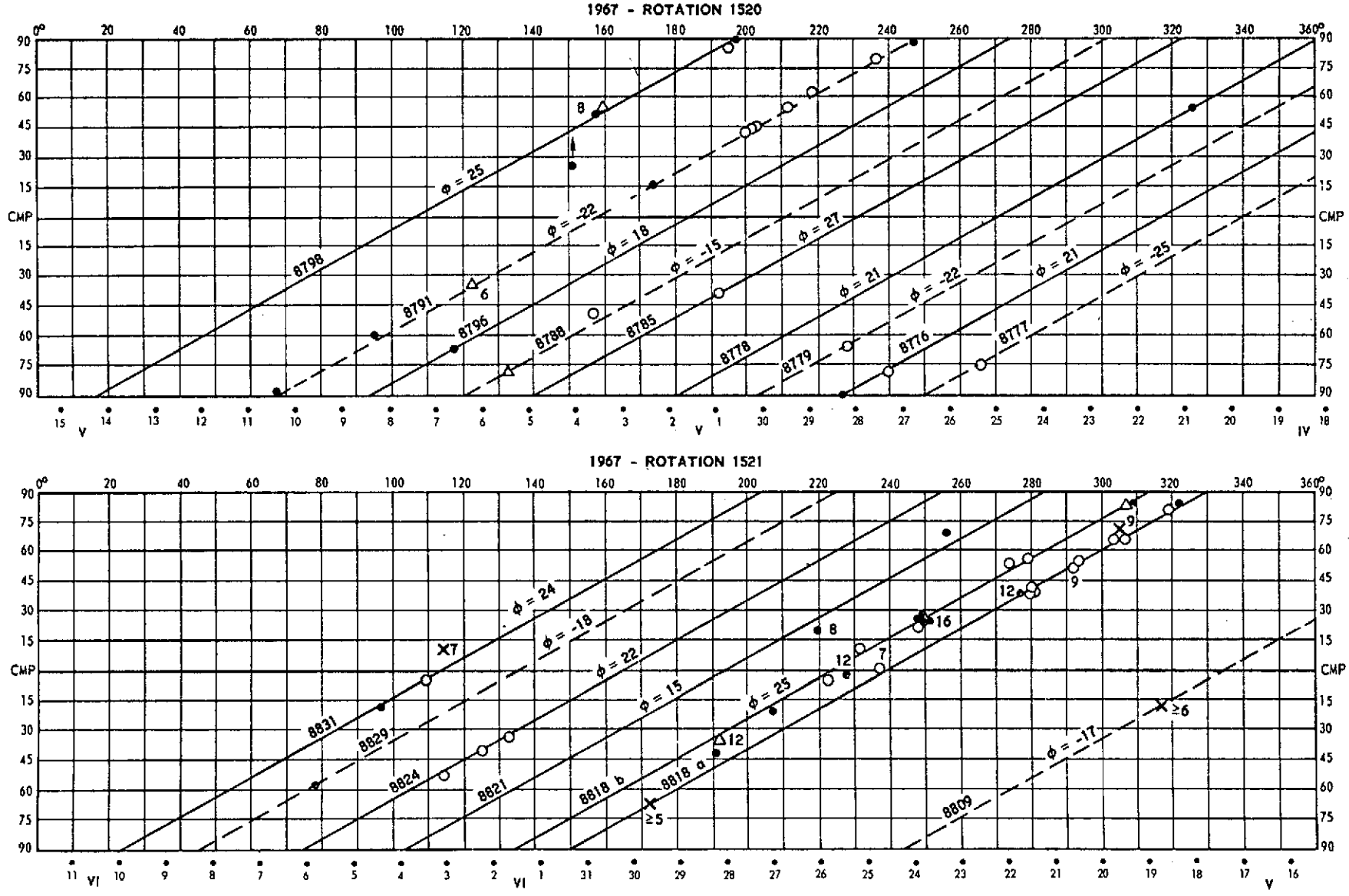
1967 - ROTATION 1520
1967 - ROTATION 1521
CMP
φ = 25
φ = -22
φ = 18
φ = -15
φ = 27
φ = 21
φ = -22
φ = 21
φ = -25
8798
8791
8796
8788
8785
8778
8779
8776
8777
φ = 24
φ = -18
φ = 22
φ = 15
φ = 25
φ = -17
8831
8829
8824
8821
8818 b
8818 a
8809

Fig. 24

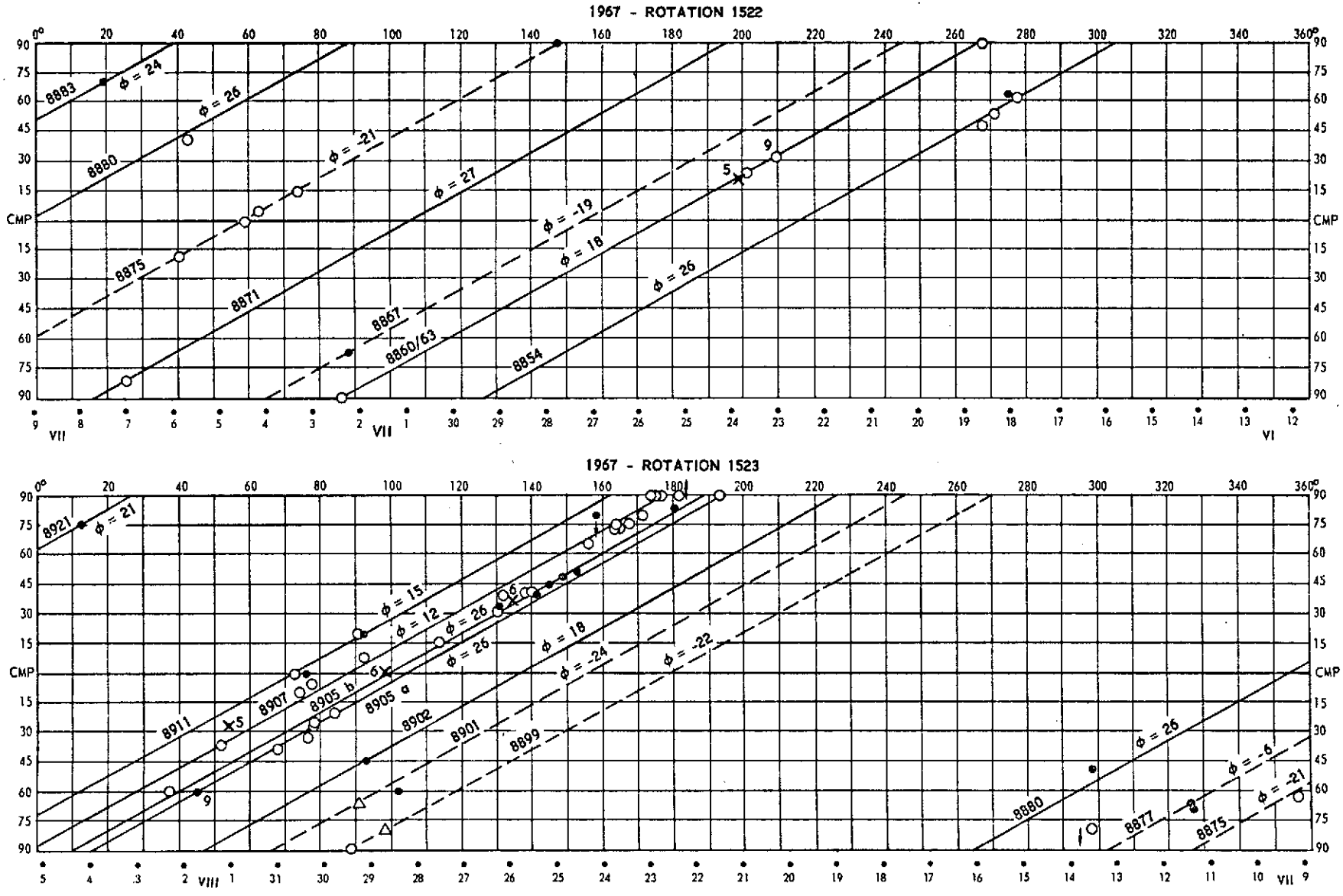
1967 - ROTATION 1522
8883
8880
8875
8871
8867
8860/63
8854
φ = 24
φ = 26
φ = -21
φ = 27
φ = -19
φ = 18
φ = 26
CMP
VII
VII
VI
1967 - ROTATION 1523
8921
8911
8907
8905 b
8905 a
8902
8901
8899
8880
8877
8875
φ = 21
φ = 15
φ = 12
φ = 26
φ = 26
φ = 18
φ = -24
φ = -22
φ = 26
φ = -6
φ = -21
CMP
VIII
VII

Fig. 25

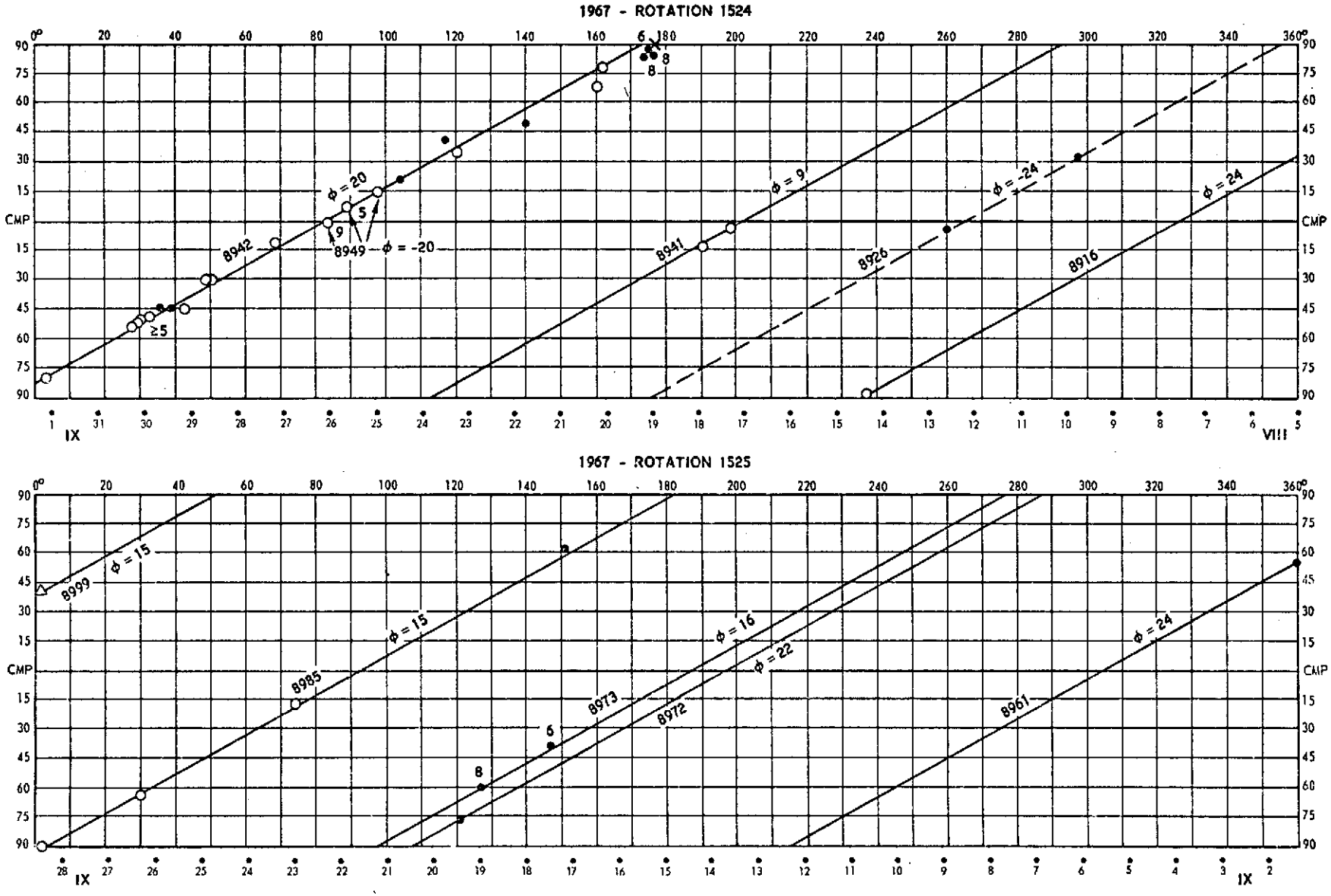
1967 - ROTATION 1524
CMP
IX
VIII
8942
8949
8941
8926
8916
φ = 20
φ = -20
φ = 9
φ = -24
φ = 24
≥5
1967 - ROTATION 1525
CMP
IX
IX
8999
8985
8973
8972
8961
φ = 15
φ = 15
φ = 16
φ = 22
φ = 24

Fig. 26

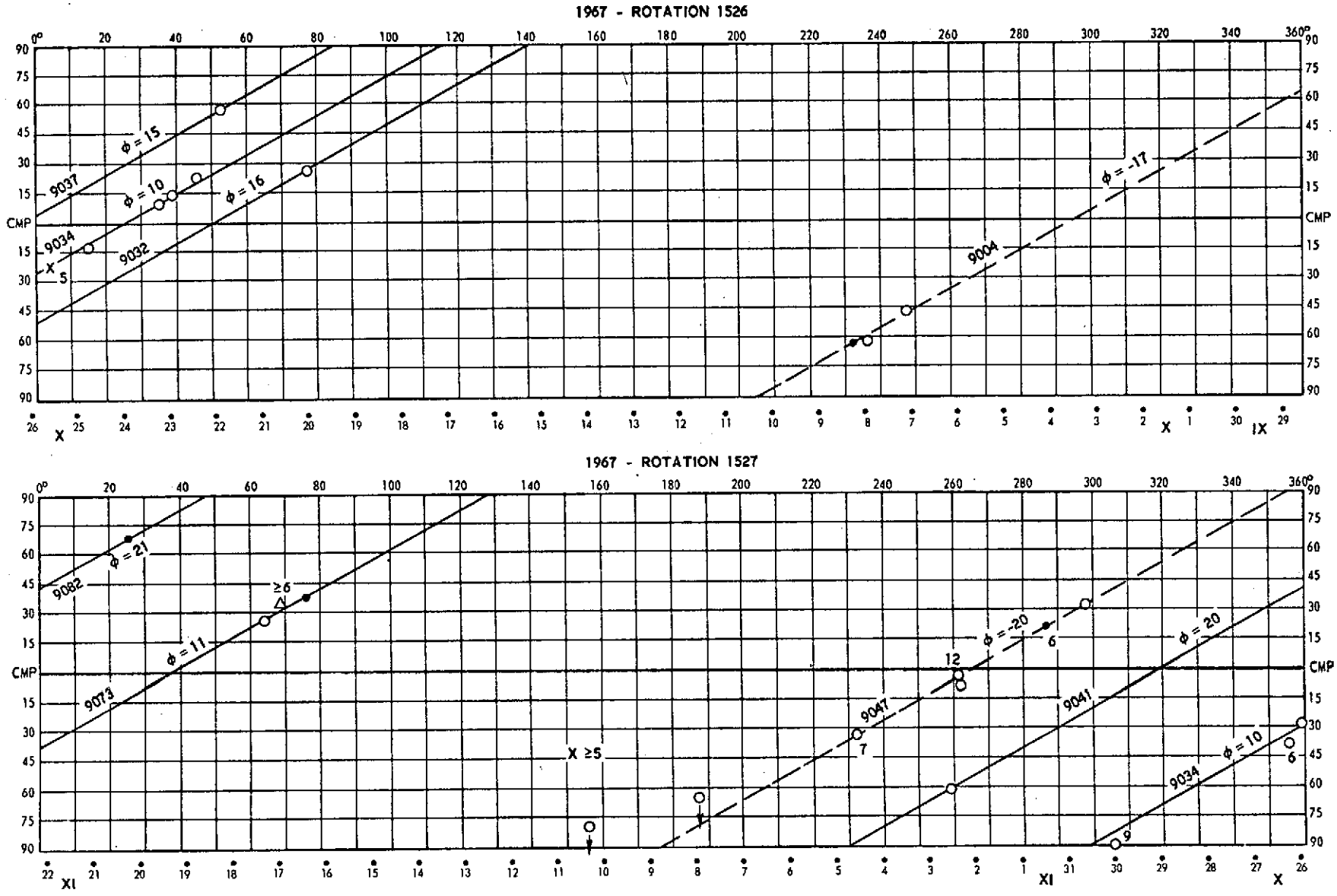
1967 - ROTATION 1526
1967 - ROTATION 1527
CMP
X
IX
XI
9037
9034
9032
9004
9082
9073
9047
9041
φ = 15
φ = 10
φ = 16
φ = -17
φ = 21
φ = 11
φ = -20
φ = 20
φ = 10
≥6
X ≥5

Fig. 27

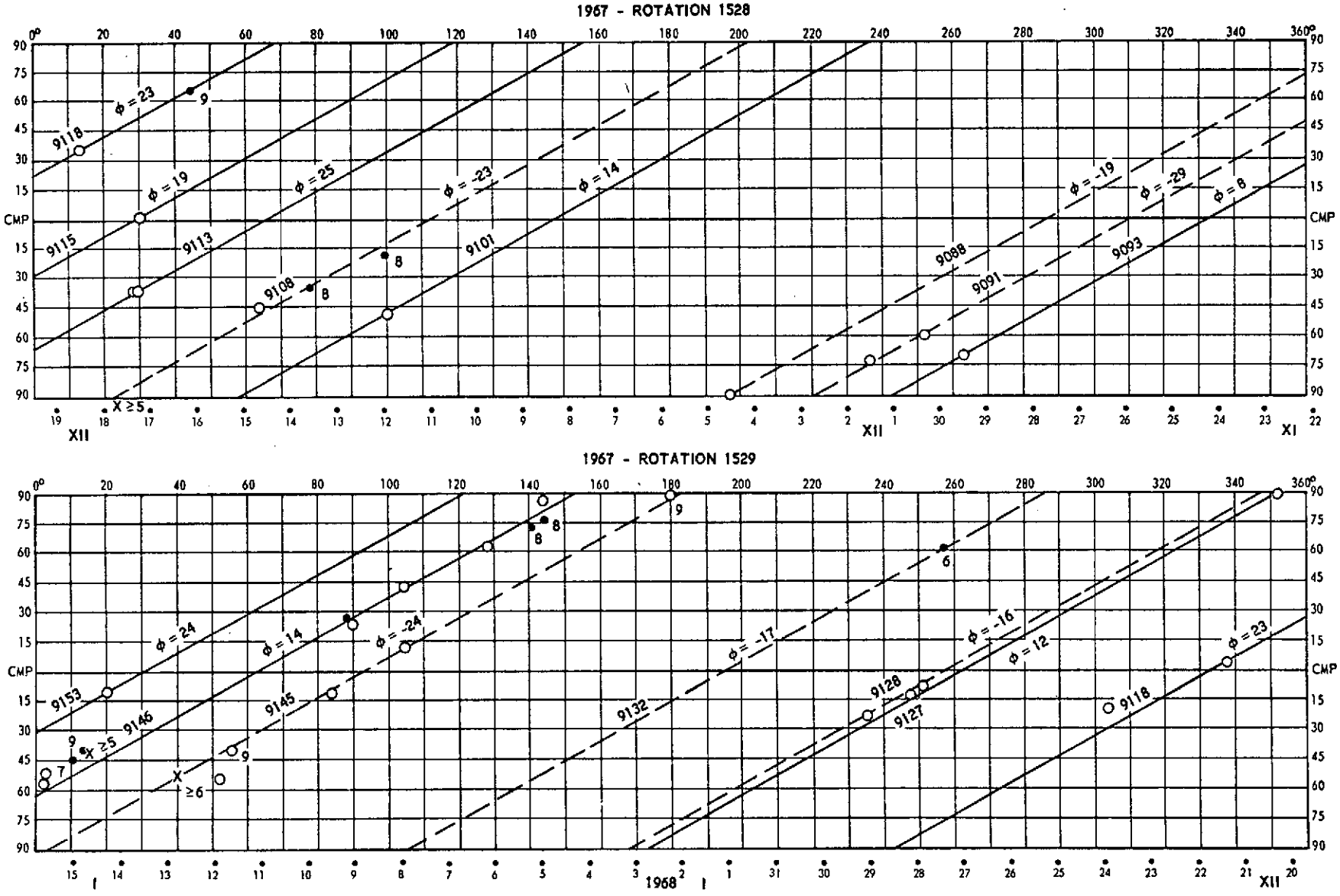
1967 - ROTATION 1528
1967 - ROTATION 1529
CMP
XII
XI
1968
φ = 23
φ = 19
φ = 25
φ = -23
φ = 14
φ = -19
φ = -29
φ = 8
φ = 24
φ = -24
φ = -17
φ = -16
φ = 12
9118
9115
9113
9108
9101
9088
9091
9093
9153
9146
9145
9132
9128
9127
X ≥5
X ≥6

Fig. 28

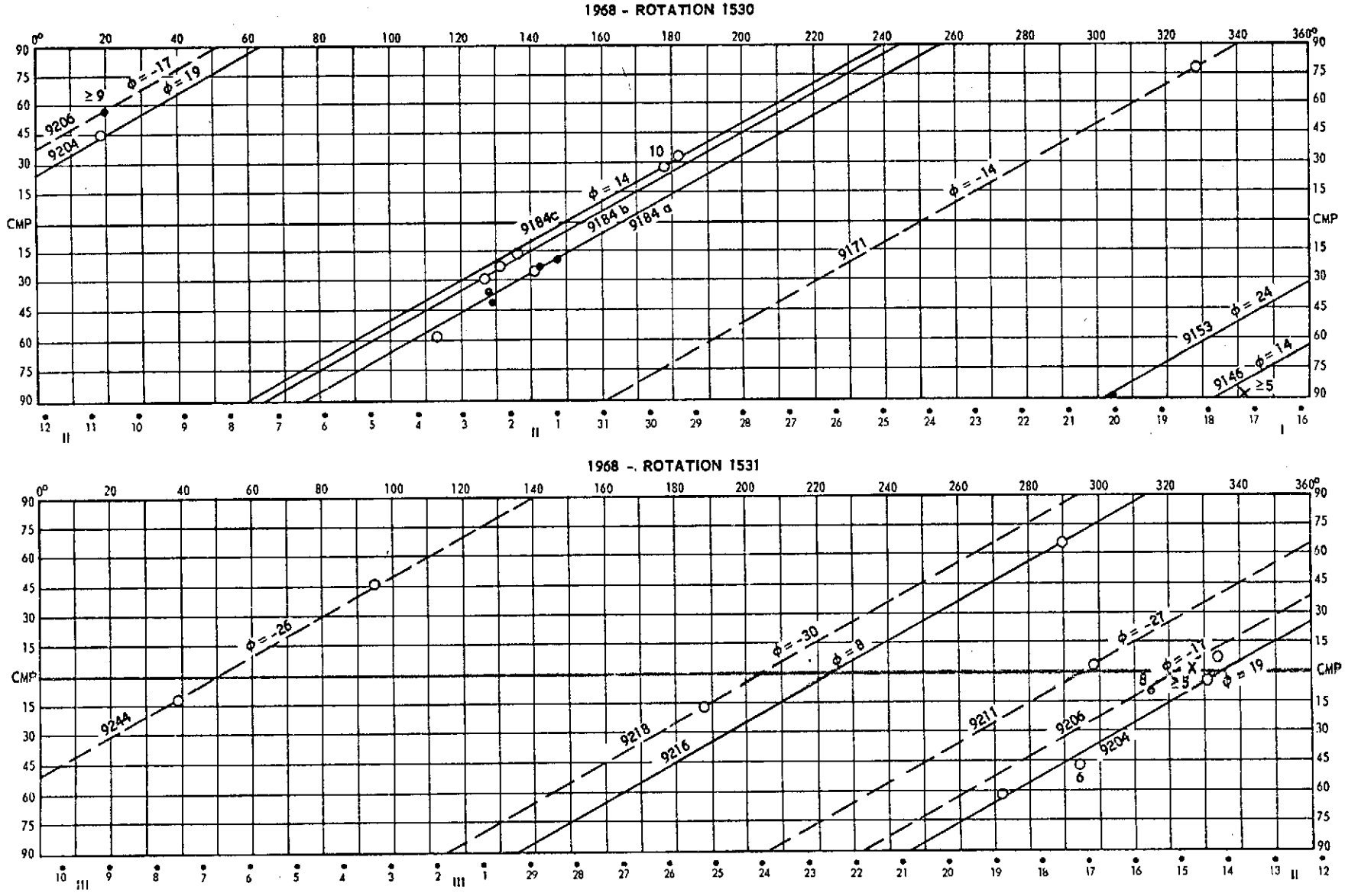
1968 - ROTATION 1530
1968 - ROTATION 1531
CMP
9206
9204
9184c
9184 b
9184 a
9171
9153
9146
9244
9218
9216
9211
9206
9204
φ = -17
φ = 19
φ = 14
φ = -14
φ = 24
φ = -26
φ = -30
φ = 8
φ = -27
φ = 19
≥ 9
≥ 5
10
8
6

Fig. 29

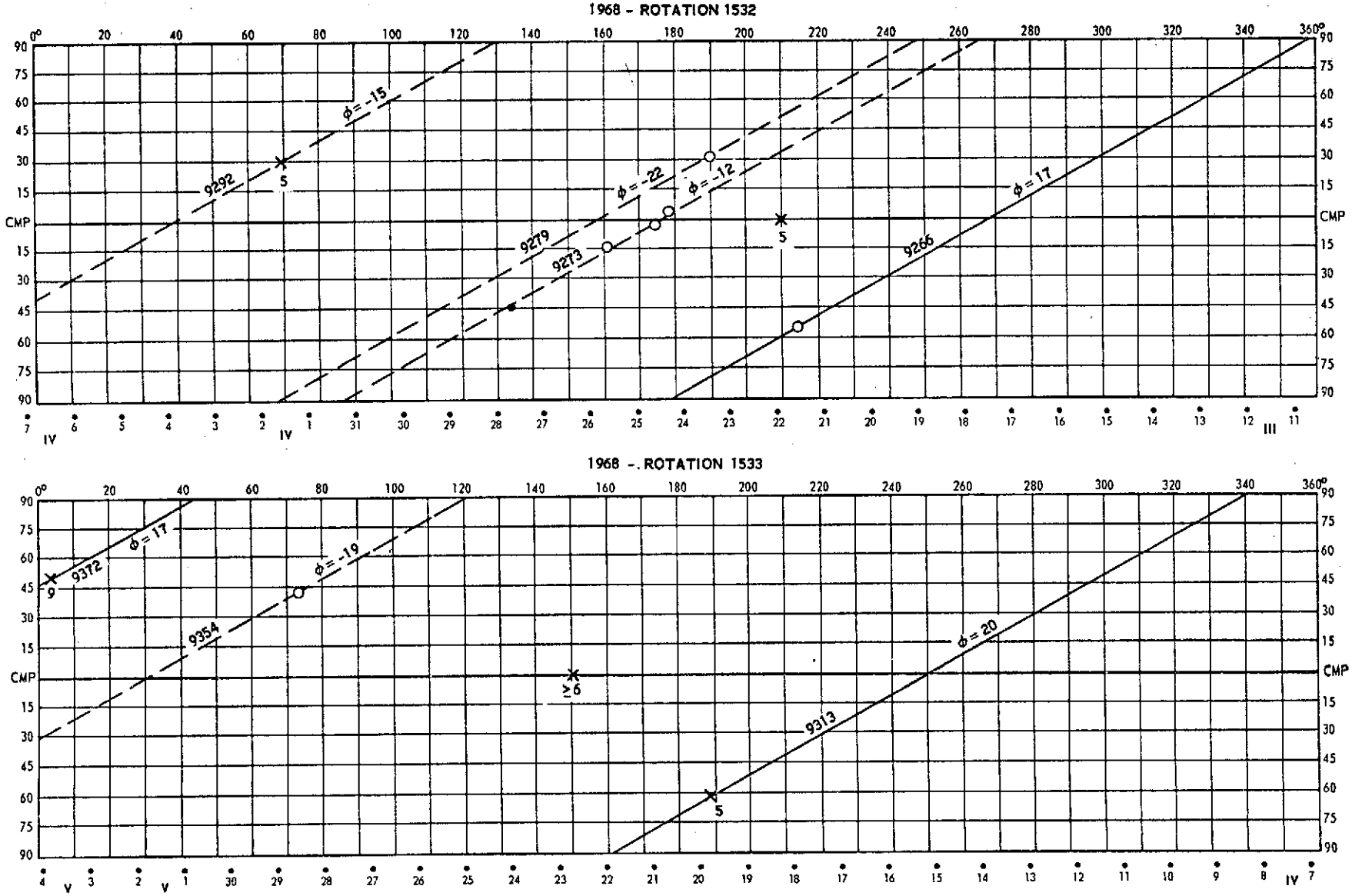
1968 - ROTATION 1532
CMP
φ = -15
9292
5
φ = -22
φ = -12
9279
9273
5
φ = 17
9266
1968 -. ROTATION 1533
CMP
φ = 17
9372
9
φ = -19
9354
≥6
φ = 20
9313
5

Fig. 30

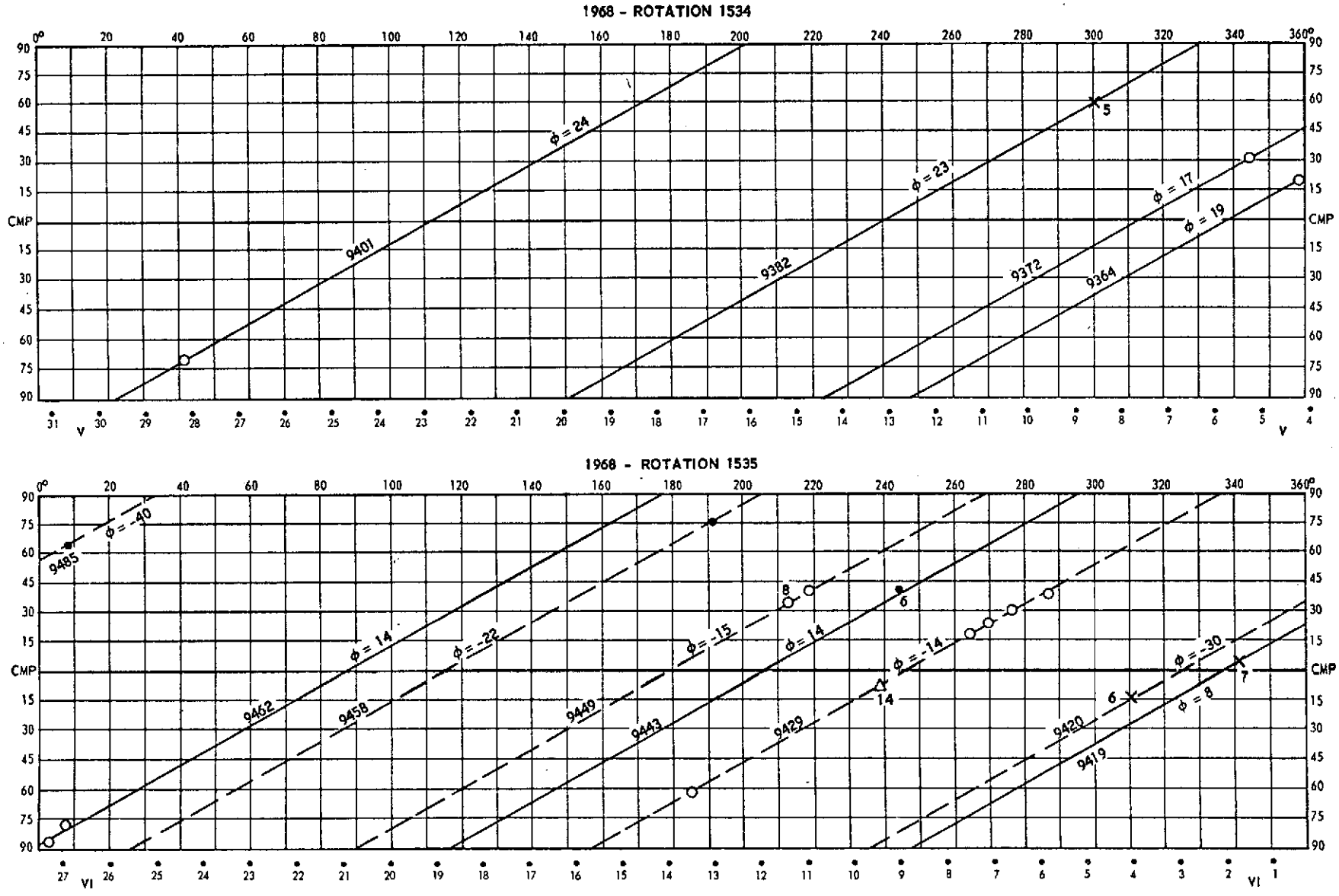
1968 - ROTATION 1534
CMP
V
φ = 24
φ = 23
φ = 17
φ = 19
9401
9382
9372
9364
5
1968 - ROTATION 1535
CMP
VI
φ = -40
φ = 14
φ = -22
φ = -15
φ = 14
φ = -14
φ = -30
φ = 8
9485
9462
9458
9449
9443
9429
9420
9419
8
6
14
7
6

Fig. 31

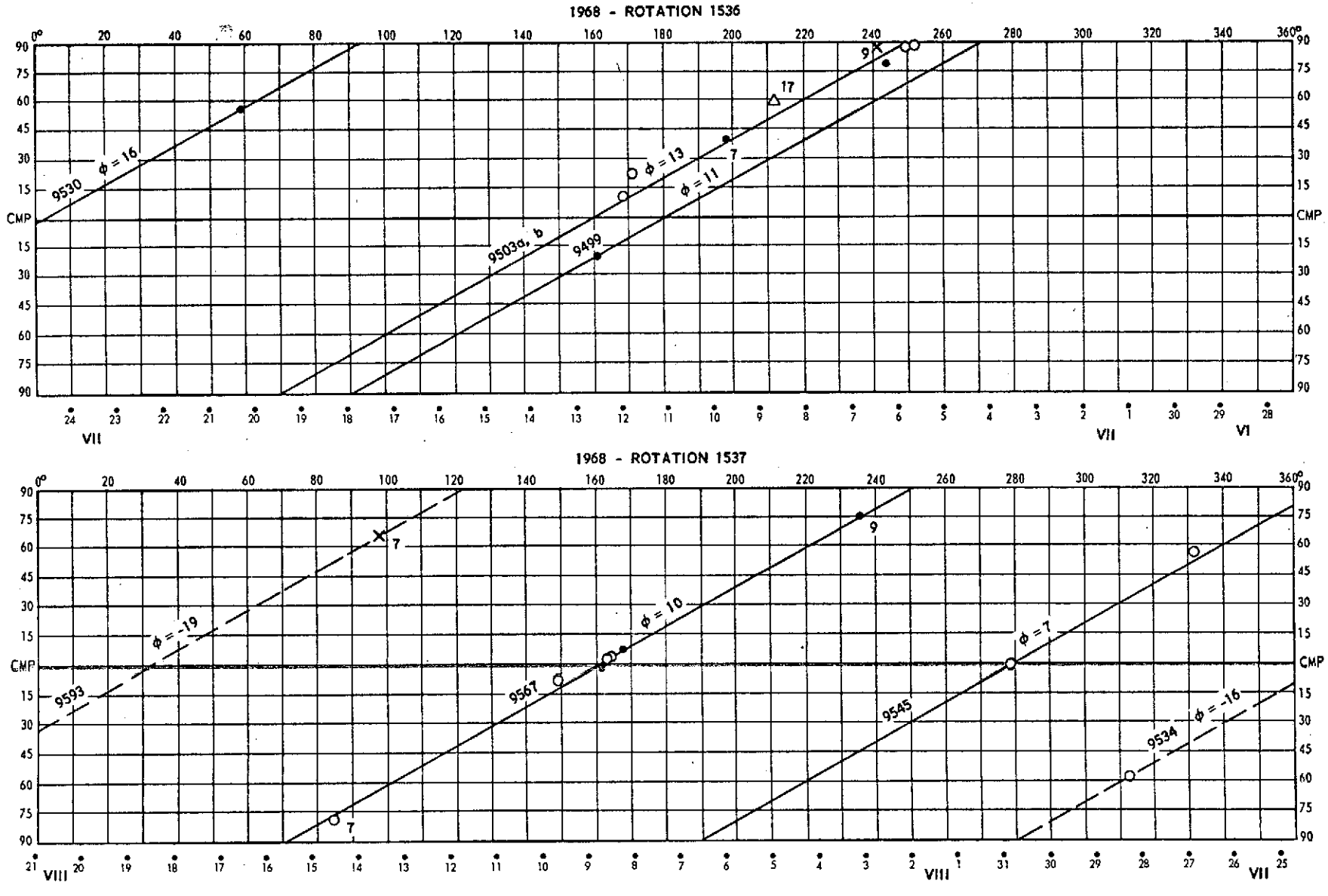
1968 - ROTATION 1536
1968 - ROTATION 1537
CMP
9530
9503a, b
9499
9593
9567
9545
9534
φ = 16
φ = 13
φ = 11
φ = -19
φ = 10
φ = 7
φ = -16
VII
VIII
VI

Fig. 32

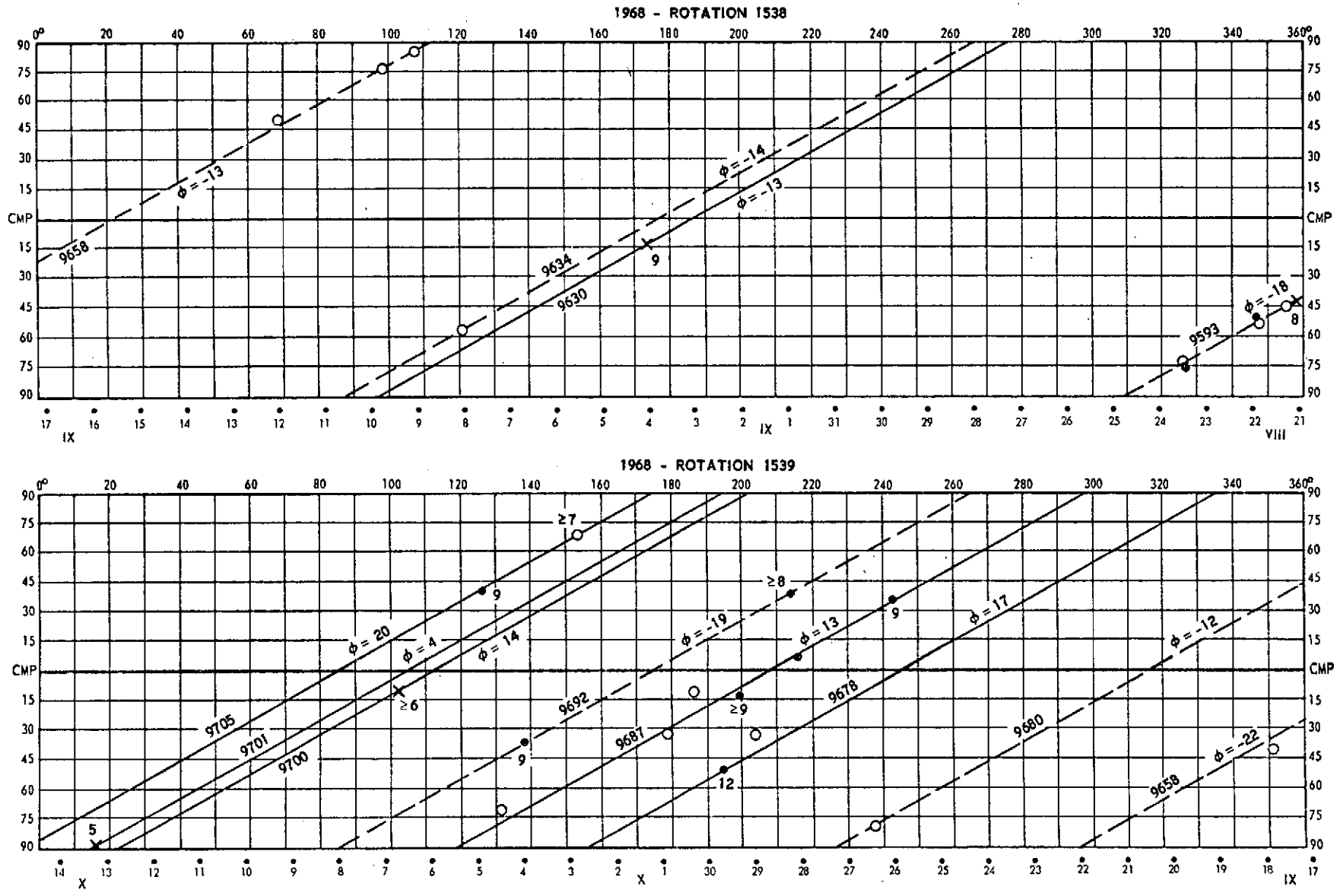
1968 - ROTATION 1538
CMP
9658
9634
9630
9593
φ = -13
φ = -14
φ = -13
φ = -18
9
8
IX
IX
VIII
1968 - ROTATION 1539
CMP
9705
9701
9700
9692
9687
9678
9680
9658
φ = 20
φ = 4
φ = 14
φ = -19
φ = 13
φ = 17
φ = -12
φ = -22
≥7
≥8
≥6
≥9
9
9
9
12
5
X
X
IX

Fig. 33